Chapter 3.2

Ice Thickness and Roughness Measurements

Christian Haas and Matthew Druckenmiller

3.2.1 INTRODUCTION

Apart from ice concentration and ice extent, which are related to the presence or absence of ice, thickness is probably the most important sea ice property, defining its quality and suitability for providing the services discussed in Chapter 2. In this chapter, basic aspects of the ice thickness distribution will be discussed, measurement methods will be presented, and applications of the methods for various users of sea ice services will be demonstrated.

Throughout the chapter, the term *ice thickness* will be used to describe the distance between the ice surface and the ice underside. This term is more objective than *ice depth*, which is sometimes used instead and seems more obvious for observers standing on the ice and wondering about what is below them. Similarly, snow thickness is sometimes referred to as *snow depth*. Definitions of ice thickness often include the thickness of snow, in which case it should rather be referred to as *total ice thickness*. Definitions for all these terms are given below (Section 3.2.2), so that one may properly define each variable and observation and avoid notation errors that may significantly miscommunicate data.

3.2.1.1 The Ice Thickness Distribution

Figure 3.2.1 shows aerial photographs of typical sea ice covers, both during the winter (left) and summer (right). It can be seen that the ice surface is covered by miniature mountain ranges, so-called ridges and rubble, which result in a considerably rough surface. As sea ice floats on the water and is generally in isostatic equilibrium, it is clear that ridge sails at the ice surface must be accompanied by ridge keels below the ice, and that the ice is considerably thicker at those locations than at the adjacent level ice. In the Arctic and even at the North Pole, the snow and upper ice layers typically melt during the summer, resulting in meltwater that collects in so-called melt ponds (Figure 3.2.1, right). Because of their low albedo, melt ponds

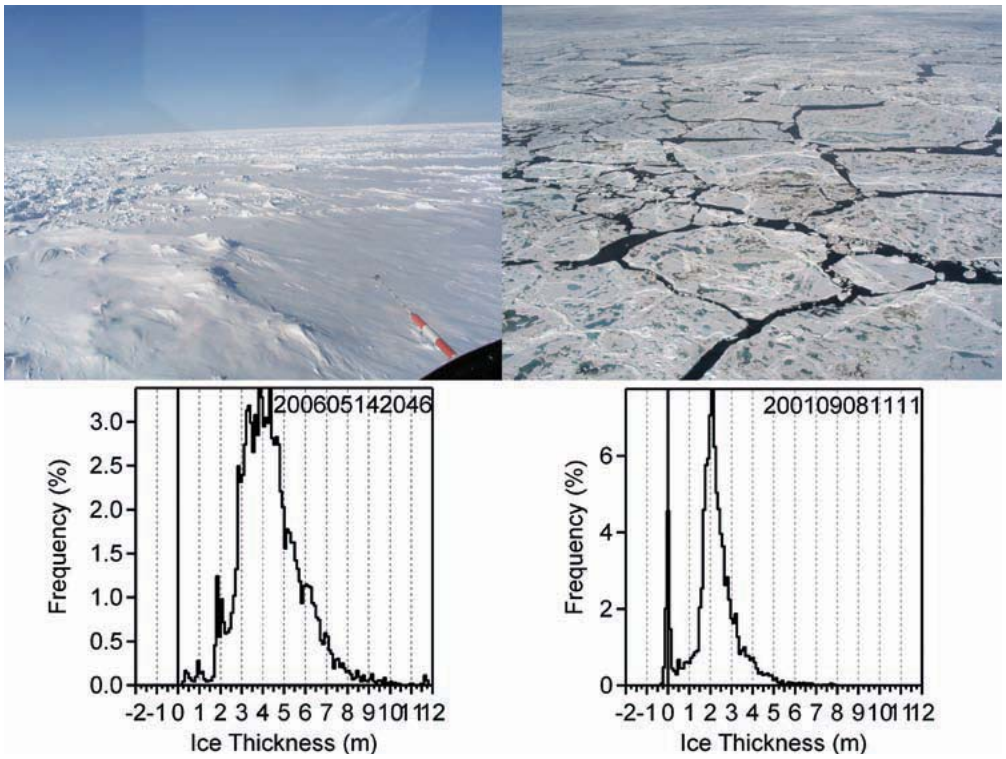

Figure 3.2.1. Aerial photographs and thickness distributions from airborne electromagnetic sounding typical of Arctic sea ice in winter (left) and summer (right), from old multiyear ice in the Lincoln Sea (left) and second- and multiyear ice in the region of the North Pole (right). See text below on aspects of airborne electromagnetic sounding for deriving these thickness distributions.

enhance local melt (Section 3.2.9.5). Due to this preferential melting, the ice is typically thinnest at melt ponds, which additionally increases the roughness of the ice.

From this discussion of small-scale thickness variability it already becomes clear that a single ice thickness measurement may not be sufficient to characterize the thickness of an ice floe. Instead, a larger number of measurements is required, and should extend across a representative section of ice, comprising both level and rough ice, and possibly melt ponds. This so-called thickness profile can best be represented by means of a histogram or thickness distribution, as illustrated in Figure 3.2.1.

The thickness distribution is defined as a probability density function g(h) of the areal fraction of ice with a certain ice thickness (Thorndike et al. 1975). The probability density function (pdf) of ice thickness g(h) is given in Equation 3.2.1 by

$$g(h)\,dh = dA(h,h+dh) / R \qquad \text{(Equation 3.2.1)},$$

where $dA(h,h+dh)$ is the areal fraction of a region R covered with ice of thickness between h and $(h+dh)$. In practice, the thickness distribution is mostly obtained

along linear profiles, and dA and R are one-dimensional, with R as the total length of the profile. g(h) is derived by dividing a frequency histogram of ice thickness data by the bin width (dh). Thus, its dimension is m^{-1}. Note that with a pdf the numerical value of each thickness bin is independent from the bin width used in calculating the histogram. This may be required if numerical values of thickness histograms are to be compared with other distributions, or are used to parameterize the thickness distribution in computer models. For most practical applications, it is sufficient to calculate the frequency distribution and to give results in fractions or in percentages.

Figure 3.2.1 shows typical thickness distributions representing the winter and summer conditions seen in the aerial photographs. The left histogram is from old multiyear ice in the Lincoln Sea north of Ellesmere Island, Canada. It possesses multiple local maxima, so-called modes, and a long tail towards thick ice. Note that there is almost no open water, as the fraction of ice with thickness 0 m is zero. In contrast, there is > 4 percent open water in the summer thickness distribution, which was obtained over second- and multiyear ice in the region of the North Pole in summer. This thickness distribution possesses only one clear mode (at 2.1 m), and its tail drops off towards thick ice considerably faster than in the example on the left.

The thickness distributions shown in Figure 3.2.1 give an accurate representation of ice thicknesses present along the surveyed profiles. They demonstrate in particular that ice thickness is mostly nonuniform, but very variable on small scales of meters to tens of meters. This small-scale variability is caused by the various and interacting processes of freezing, melting, and deformation. In fact, the thickness distribution bears information on the history and relative importance of these processes. Sea ice is only a relatively thin layer on the water, and thus rapidly responds by motion or drift to external forces exerted by winds and currents. The resulting forces are often nonuniform due to the divergence of winds and currents, and due to internal forces of the ice or the presence of obstacles like islands or coasts. Therefore, the ice cover frequently opens in divergent regions to form leads and polynyas, or ice floes collide with each other in convergent regions. If resulting forces exceed the fracture toughness of the ice, the ice breaks and ice blocks and fragments are piled above and below the adjacent ice to form pressure ridges and rubble fields (Figure 3.2.2 and animation on accompanying DVD). In contrast, new ice growth commences in open water once it is exposed to the cold air, adding regions of thin ice of variable thickness to the ice cover. This thermodynamically grown ice is mostly undeformed and level, while dynamically formed, deformed ice is typically very rough.

Most ice covers consist of larger regions of thermodynamically grown level ice, intersected by smaller regions of dynamically formed, deformed ice. This can be seen in the thickness distribution from the region of the North Pole, for example (Figure 3.2.1). The strong mode of 2.1 m indicates the thickness of the majority of

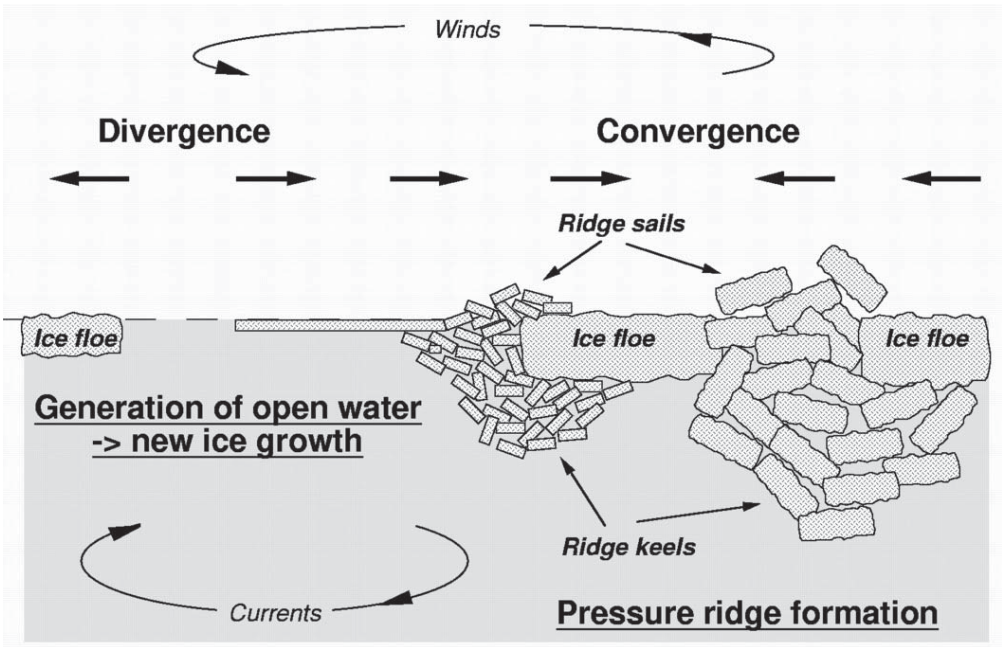

Figure 3.2.2. Illustration of the different dynamic and thermodynamic processes contributing to the development of the ice thickness distribution of a sea ice cover.

the ice, which in this case was level second-year ice. As such, it is an indication of thermodynamic growth conditions (freezing and melting) throughout the history of that ice cover. Changes in thermodynamic growth, for example due to the seasonal cycle or long-term climate changes, would leave the shape of the distribution almost unchanged, but would result in shifts of modal thickness towards thinner or thicker ice. In contrast, the tail of the distribution represents the thickness and amount of deformed ice, and is therefore a measure of the intensity of deformation throughout the evolution of the ice cover. The fraction and thickness of deformed ice is affected by changes in ice motion, which can result from changes in atmospheric circulation patterns or ocean currents. It is also affected by the age of the ice cover, since more and more ice is typically added to it the longer it evolves. However, it is important to note that the thick ice of ridges is also subject to preferential ablation during the summer (Perovich et al. 2003).

These contrasts are clearly seen when comparing the second-year thickness distribution in Figure 3.2.1 (right) with the old multiyear ice thickness distribution in Figure 3.2.1 (left). The latter is characterized by multiple modes representing various classes of young ice and multiyear ice, as well as by a well-developed tail with significant amounts of deformed ice thicker than 10 m.

The discussion of Figure 3.2.1 has shown that only a description of the complete thickness distribution can reveal the different aspects of an ice cover's developmental history and the importance of the underlying dynamic and thermodynamic

growth processes. For example, the mean thicknesses of 4.33±1.48 m (± one standard deviation) and 2.22±0.80 m resulting from the two distributions in Figure 3.2.1 bear no information about the occurrence and fractions of individual ice types (with modal thicknesses of 0.5 m, 1.0 m, 1.9 m, 3.9 m, 4.4 m in the Lincoln Sea, and 0.0, and 2.1 m at the North Pole, respectively), open water, or deformed ice. However, the standard deviation of a mean thickness indicates the range of occurring thicknesses and can therefore serve as a measure for sea ice roughness as well.

While this discussion was mostly focused on regional scales from meters to tens of kilometers, it should be noted that the same dynamic and thermodynamic processes also act on basinwide or hemispheric scales. For example, the long-term mean drift systems of the Transpolar Drift and Beaufort Gyre in the Arctic Ocean remove ice quasi-permanently from the Siberian Arctic and move it across the North Pole towards the coasts of Canada and Greenland. As a result, polynyas and thin ice prevail along the coasts of Siberia, while the thickest ice is found off the coasts of North America. Similar conditions are observed in the Southern Ocean, where for example the Weddell Gyre pushes ice against the Antarctic Peninsula, resulting in ice almost as thick as observed in the Arctic.

3.2.2 INTRODUCTION TO MEASUREMENT TECHNIQUES IN RELATION TO VARIOUS SEA ICE SERVICES

It is clear that a full description of the ice thickness distribution is far beyond the aims, capabilities, or requirements of many activities related to the various sea ice services. Table 3.2.1 provides an overview of the services, and of the different relevant temporal and spatial scales on which thickness information is required or relevant. From these, it becomes already clear that not every method discussed below is suitable to provide the required data.

Table 3.2.1 is contrasted by an overview of the available and most frequently used thickness measurement methods in Table 3.2.2. These methods will be described in detail in the sections below. Suitable thickness measurement methods can be identified by matching the relevant and achievable spatial and temporal scales and resolutions. Some examples for the application of certain methods in using various sea ice services are given in Section 3.2.9. The values in Table 3.2.2 are only rough estimates. Explanations for the accuracy are given in the sections below. Here, only the accuracy in the actually observed variable is given, for example surface elevation in the case of altimeter measurements, or total thickness in the case of electromagnetic (EM) sounding. It should be noted that with any of the methods described below, accuracy varies with spatial scale, ice type and roughness, and even ice thickness itself. For example, the accuracy of drill-hole measurements degrades for ice thicker than 10 m or so, and EM sounding strongly underestimates maximum ridge thicknesses, while possessing high accuracy over level ice. Spatial resolution and temporal resolution are stated for the most common applications.

Table 3.2.1 Sea ice system services and related activities that may benefit from ice morphology and thickness measurements *(from Eicken et al. 2009)*

Sea ice services and related activities[a]	Examples of the role of ice morphology and thickness	Scales of relevance [b]	
		Spatial (m)	Temporal
Regulator of arctic and global climate	Partially control albedo; related to the probability of first-year ice surviving the summer melt season	0.01–100,000	days–years
Hazard for marine shipping and coastal infrastructure	Key variables of importance when deciding whether to navigate through icy waters; determines the load imparted by an ice floe impacting an offshore structure	1–100	minutes–years
Stabilizing element for near-shore infrastructure	Contribute to whether or not the ice is stably grounded in the landfast ice zone or able to withstand pressures from the adjacent ice pack	1–100	hours–months
Subsistence activities on or from the ice			
On-ice travel and a platform for industrial activities	Central to determining load-bearing capacity; surface roughness relates to trafficability (see Section 3.2.9)	0.1–100	hours–months
Sea ice–based food webs and ice as a habitat	Related to the ability of marine mammals, such as polar bears and ice seals, to find suitable conditions for denning	0.1–1000	months–years
Reservoir and driver of biological diversity	Control the amount of light available to biota within and under the ice	0.1–1	months–years
Oil spill response	Partially determine pathways and reservoirs for oil spilled beneath sea ice	0.1–100	hours–days

[a] *Categories adopted from Section 2, Table 1, of Eicken et al. (2009).*

[b] *These spatial and temporal scales relate to the importance of ice morphology and thickness to the listed sea ice services. Other variables may be of importance on different scales. For example, permeability on subcentimeter scales is important to responding to oil spilled beneath ice.*

Clearly, drill-hole measurements could be performed with higher resolution, for example, but there is a limit of feasibility, especially as the destructive nature of this technique is considered. Similarly, the spatial coverage is given as that most commonly achieved. Of course, drill-hole measurements could be extended to cover larger regions, as more efficient modes of transportation are explored, or airborne surveys could be extended by using larger planes or fuel caches on the ice. Real-time capability is very important for many sea ice services, as can be seen by small temporal scales listed in Table 3.2.1. Also, the numbers of individuals or institutions using methods are only rough estimates. They are meant to represent the number of researchers who can actively perform or process measurements rather than only

Table 3.2.2 Overview of ice thickness and roughness measurement techniques and their various characteristics. Variables represent most common applications and present technical feasibility, and only rough quantitative estimates.

Method	Accuracy of observed variable (m)	Spatial resolution (m)	Temporal resolution	Spatial coverage (km)	Real-time capability	Applied by N individuals/ institutions
Drilling	0.02	0.5–5	weeks–years	0.1–10	Yes	>100
EM sounding (ground-based)	0.1	5	weeks–years	0.1–10	Yes	20
Laser surveying	0.02	0.5–5	weeks–years	0.1–10	Yes	10
DGPS surveying	0.05	0.5–5	weeks–years	0.1–10	Yes	10
IMBs[a]	0.1	n/a	hours–days	local	Yes	10
ULS[b] submarine	0.1	1–5	years–decades	500-5000	No	2
ULS[b] moored	0.1	5–50	minutes–hours	Local, or depending on ice drift speed (tens to hundreds of kilometers)	Not yet	20
AEM[c]	0.1	3–5	weeks–years	10–100	Yes	6
Airborne laser profiling	0.1	0.2–5	weeks–years	10–1,000	No	10
Satellite laser altimetry	0.07[d]	170–25,000[d]	hours–days–half-yearly[d]	1,000–10,000	No	5
Satellite radar altimetry	0.07[d]	330–100,000[d]	hours–days–weeks–months[1]	1,000–10,000	No	5

[a] *Ice mass balance buoy (IMB)*
[b] *Upward-looking sonar (ULS)*
[c] *Airborne electromagnetic sounding (AEM)*
[d] *Depending on spatial and temporal averaging*

use the final data. For example, many scientists have used ice thickness data from submarine upward-looking sonar (ULS) which are freely available through the Internet. However, only two researchers or institutions, namely in the United States and United Kingdom, can at present contribute to future mission planning and performance, if at all. Similarly, the acquisition and processing of satellite altimetry data is dependent on the availability and orbits of satellites, and processing often requires close insights into satellite system parameters and access to auxiliary data. These, as well as the planning of future satellite missions, are only available to very few research groups.

The next sections provide overviews of the most commonly used methods of ice thickness and roughness surveying. These are ordered from the most simple towards the most advanced techniques, with less emphasis on the latter as they

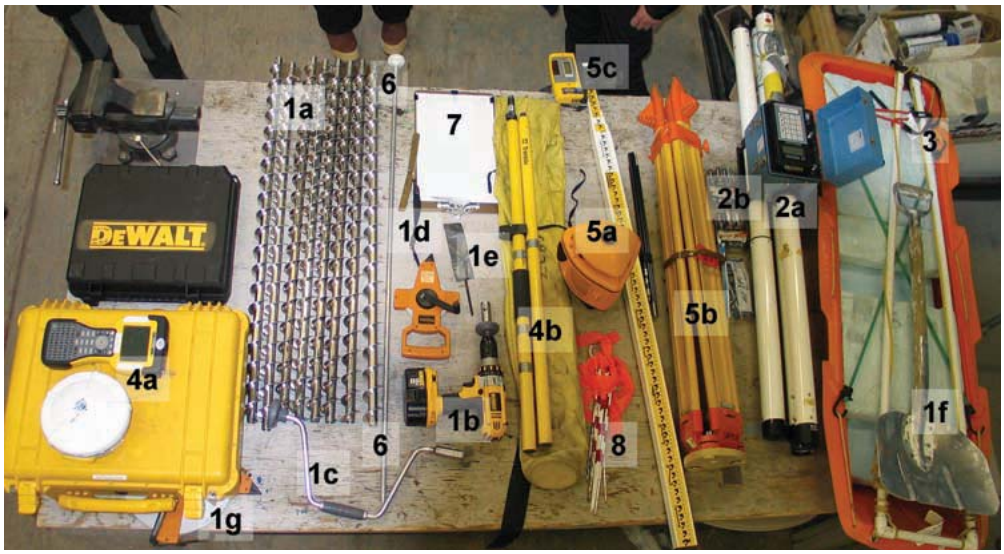

Figure 3.2.3. Assemblage of different instruments for simple ground-based thickness measurements (one or several of those may be used):

1. Thickness auger with numerous drill extensions (a; drill bit not visible), with cordless power drill (b), emergency hand brace (c), thickness gauge (d), button release tool (e), shovel (f), and 60 m ruler tape (g).
2. EM31-MK2 ground conductivity meter with onboard data logger (a), with spare batteries (b).
3. Pulka sledge for transport of equipment or dragging of EM31.
4. Differential GPS antenna and data logger (a), and range pole (b).
5. Rotating laser (a) with tripod (b) and telescopic range pole with laser detector (c).
6. Snow thickness meter stick.
7. Clipboard for paper sheets.
8. Pegs for marking field sites and fixing ruler tapes.

typically require significant expert knowledge and heavy logistics. There are several trade-offs between those methods. The most simple measurements like drilling are often the most accurate, but progress is slow, and measurements require hard work. Therefore, they are mostly also spatially limited. In contrast, advanced methods like airborne or satellite altimetry provide repeat data over large regions. However, their accuracy can be questionable, and logistical support and data access is often limited to a few individuals.

Figure 3.2.3 shows all the equipment required to perform drill-hole and ground-based EM thickness measurements, as well as laser and DGPS surveying—four techniques discussed in this section. This equipment can easily be assembled and taken by almost anyone to the ice to gather a thorough thickness and roughness data set.

More information on details of measurements can also be found in the *Handbook for Community-Based Sea Ice Monitoring* (Mahoney and Gearheard 2008).

That book focuses on drill-hole and hotwire measurements that can easily be performed by nonexperts. This chapter will not discuss visual observations of ice thickness, which, for example, can be performed from icebreakers when ice floes turn and are pushed up along the hull, revealing their cross-sectional profile, which can then be compared with a scale. However, it should be noted that this method is quite important, and has contributed much knowledge, particularly of the large-scale thickness distribution in the Southern Ocean, more than is available from any other method to date (Worby et al. 2008). It is also further discussed in Chapter 3.12. The chapter will not address satellite remote-sensing methods other than altimetry, although the thickness of thin ice can sometimes be successfully retrieved from thermal infrared imaging. Imaging remote sensing methods are further discussed in Chapter 3.15.

3.2.3 DRILLING

Figure 3.2.4 defines the most important variables commonly referred to with respect to ice thickness. Ice thickness is the distance between the ice underside (or ice-water interface) and the ice surface (or snow-ice interface), while snow thickness is the distance between the snow-ice interface and the snow surface. Their sum is referred to as *total thickness*. *Freeboard* is the height of the ice surface above the water level, while *surface elevation* or *snow freeboard* are commonly used to describe the height of the snow surface above the water level. *Draft* is the depth of the ice underside below the water level. These variables do not only yield information on the overall thickness or mass of ice and snow, but ratios of freeboard and thickness, for example, can also be used to study the isostasy of the ice, and to calculate the densities of ice and snow. This principle is utilized by recent satellite altimetry missions like ICESat and CryoSat to derive ice thickness from measurements of sea ice surface elevation or freeboard (see below).

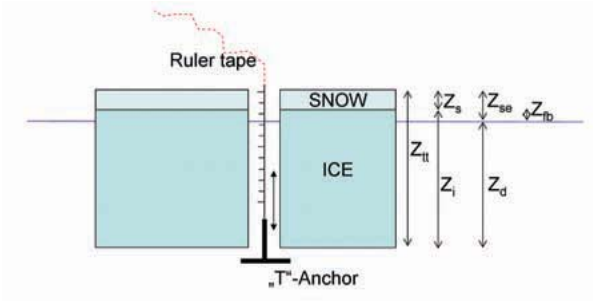

Figure 3.2.4. Measurement of total thickness (Z_{tt}), ice thickness (Z_i), snow thickness (Z_s), surface elevation (Z_{se}), draft (Z_d), and freeboard (Z_{fb}) by means of a thickness gauge (ruler tape with T-anchor) in a drill-hole.

All these variables can be measured with drill holes through the ice. In the drill hole, the water level provides a reference datum for observations of draft, freeboard, and surface elevation. Note that only three variables have to be measured, and that all other variables can be calculated by subtraction or addition from those measurements.

Two different means are commonly used to drill holes though the ice: either mechanically by means of a motor-driven ice auger or thermally by means of a steam or hot-water drill.

Motor-driven ice augers are available with various metal flight diameters between 5 and 25 cm. With increasing diameter, drilling becomes increasingly difficult, and more engine and man power are required to drill through thicker ice. An ice corer can also be used to drill a hole (see Chapter 3.3). For extensive measurements, 5 cm diameter auger flights are most widely used, as for example manufactured by Kovacs Enterprises Drilling Equipment Inc. (see photos in Figures 3.2.3 and 3.2.5). These stainless-steel flights are 1 m long and join one to another via a push-button connector, which allows for quick connection of one auger section to another. This method of assembly means that there are no pins or connector bolts to lose or care for and no bolts on which clothing can snag. At the lower end of the lowest flight, a 5.1 cm wide ice-cutting bit is used for the actual drilling.

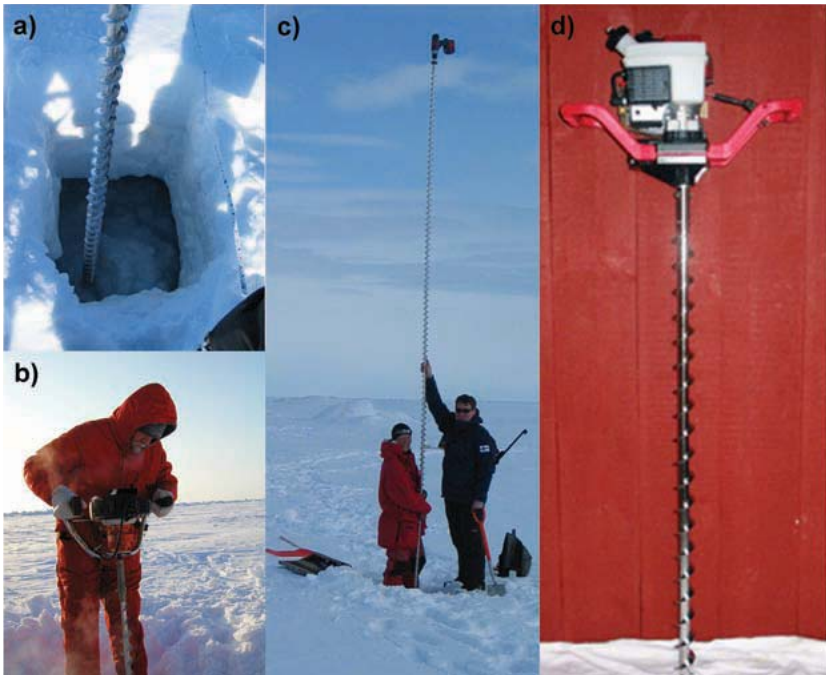

Figure 3.2.5. Equipment and procedures for mechanical ice thickness drilling. (a) Auger flights penetrating into the ice through a snow pit; (b) a two-stroke gas engine with custom-made handle bars; (c) Thick ice (>5 m) drilled with a battery powered drill; and (d) Kovacs Enterprise flight and gas power head.

Augers can be powered by two-stroke gas engines or electric power drills. Recent high-end 18 VDC cordless electric hand drills are powerful enough for most applications, and batteries may last for 30 to 50 drill meters. Drilling rates of 1 m in 15 to 20 seconds are achievable with most power drills. If one wishes to turn the augers by hand, a hand brace can be used (Figure 3.2.3).

For ice thicknesses between 1 and 2 m, it is convenient to start the drilling off with 2 m of flights, if the driller is tall enough to hold the system and safely reach the power head at > 2 m elevation. If the ice is thicker than 2 m, after every meter of drilling the drill has to be removed from the upper flight with the flights still remaining in the hole, and another extension can be inserted between the uppermost flight and the drill. By this, multiyear pressure ridges up to 24 m thick and grounded ice islands up to 23 m thick have been drilled. However, note that one flight weighs approximately 1.5 kg, and therefore the equipment becomes successively heavier and harder to manage.

When using a drill with a chuck, instead of a pin, the weight of numerous auger flights may become too heavy for the drill's chuck to hold. For this reason it is important for the bit that connects the uppermost auger flight to the drill's chuck to have a disk (rubber or metal) that is of a greater diameter than the hole (see Figure 3.2.3) in order to prevent the flights from being lost under the ice if the bit happens to slip out of the chuck.

Therefore, over thick and deformed ice thermal drills are sometimes used instead. With these, hot water or steam is generated by boiling water in a reservoir, and pumping it under high pressure through a hose into a metal rod with a typical diameter of 3 cm (Figure 3.2.6). The hot rod tip as well as the steam melt the ice at and below the tip, allowing the rod and hose to easily enter vertically into the slowly forming and deepening hole. Drilling progress is comparable to mechanical drilling, but the hose is lighter and much easier to use. The boiler and pump are usually powered by fuel or kerosene. A water reservoir, typically filled with water obtained from under the ice through a drill hole, is required for steam generation.

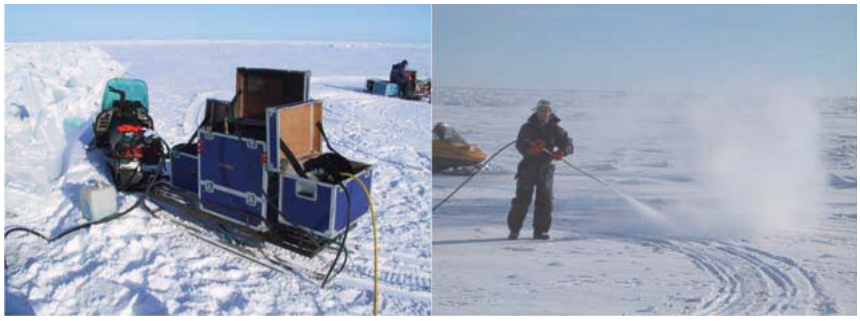

Figure 3.2.6. Operation of hot water drill comprising of a generator, pump, boiler, and hose set up on a sledge (left). A stainless-steel drill rod is used to direct the hot steam under pressure vertically into the ice (right; Photo courtesy Pekka Kosloff).

Custom-tailored hot-water drills are manufactured by Kovacs Enterprise Inc. as well. Their geometrical dimensions of 40 × 50 × 50 cm^3 and typical weights of > 70 kg require heavier logistics for transport and operation. Therefore, they are often set up at only one place (e.g., close to a pressure ridge) and then a wide area is reached by means of a 50 m long hose.

With both drilling methods, complete penetration of the ice is easily felt as the drill falls freely into the water underneath. Before making any measurements, shavings around the drill hole should be carefully removed such that the original ice or snow surface is well visible. Now, the depth of the water level can be easily determined in the drill hole with respect to the ice surface, and all parameters can be measured very accurately within 2–5 cm with a thickness gauge (Figures 3.2.3 and 3.2.4, and video on accompanying DVD). The gauge consists of a ruler tape and a foldable T-anchor, which is lowered through the hole and then pulled up until the T-anchor catches the ice underside (Figures 3.2.3 and 3.2.4). Note that the narrow holes of thermal drills require a slim thickness gauge. If none is available, thickness has to be measured according to the known length of hose inserted into the ice before the instant when it melts through the ice-water interface indicated by a sudden fall. This may cause significant measurement errors.

Depending on the character of the snow (thickness, hardness), one can either drill through the snow or remove it before drilling. Snow thickness is usually measured with a meter stick or ski pole with a glued measuring tape by ramming it vertically into the snow until it encounters the underlying snow-ice interface. With metamorphous snow, the stick has to be rammed firmly several times to confirm the penetration to the hard ice surface (see Chapter 3.1). In any case, care should be taken not to disturb the original snow surface for measurements of total thickness or surface elevation.

Figure 3.2.7 shows a typical ice thickness profile obtained by mechanical drilling as described above (black lines). The profile is 400 m long and extends over both level and deformed ice. A point spacing of 5 m was chosen to properly sample the roughness of the deformed ice. Less spatial resolution would have been required to sample the very uniform level ice sections. However, the chosen point spacing should always be equidistant to allow calculation of representative statistics. It can also be seen that in this case 400 m was long enough to sample at least two zones of deformed ice, and to verify that the adjacent level ice was of the same thickness throughout, indicating the same age and origin of the ice along the whole profile. Note that snow thickness is generally larger over the deformed ice, as the roughness of ice blocks and ridge sails retains more snow during wind-redistribution events (see Chapter 3.1). In the example of Figure 3.2.7, drilling was performed by two people while a third did the actual measurements and wrote them into a notebook. The whole drill-hole survey of 81 holes was completed in approximately six hours. Overall, a total thickness of 194 m of ice was drilled, and 20 m of snow measured. Mean ice and snow thicknesses along the profile were 2.15±0.84 m (± one standard

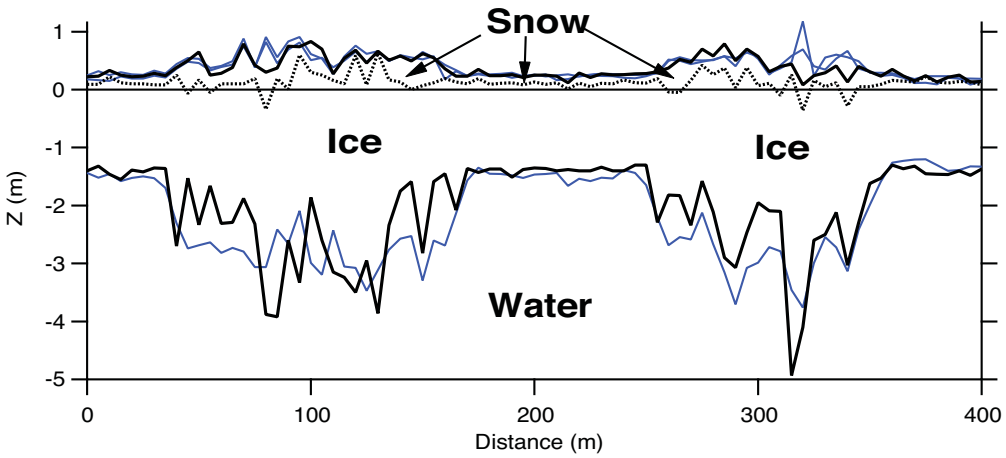

Figure 3.2.7. 400 m long ice thickness profile obtained by drilling with a point spacing of 5 m, on first-year ice at Barrow, Alaska. Z = 0 m represents the water level, and black lines indicate ice draft and surface elevation (solid), and freeboard (stippled). Blue lines show draft from ground-based EM sounding and surface elevation from laser and DGPS surveying (see below).

deviation) and 0.25±0.17 m, respectively, and their modal thicknesses were 1.5 and 0.15 m, respectively.

It should be noted that these results are only valid for this specific 400 m long thickness profile. Due to the small-scale roughness and variability, particularly in the deformed ice zone, the mean values will change when more data are added. However, the modes of the thickness distribution are very narrow and significant, and will not change as long as the profile extends over ice of the same origin and age. In general, the length of a planned thickness profile and the measurement point spacing will depend on the actual purpose of the measurement, and if regional or local data are required. Two-to-five-meter spacing is required to fully resolve the small-scale roughness due to rafting and ridging, although one would need an even finer resolution to detect very small-scale roughness. Note however that drilling is a destructive method, and the original ice underside could be easily disturbed if a drill-hole spacing of 0.1 m would be chosen, for example. A wider spacing might be chosen if regional results are of more interest, or if the ice is very level and uniform. Additional notes or photos should be taken to characterize the ice in general, and should be taken into account when interpreting the data later.

As drilling can generally be applied by anybody and is most accurate, much of our information about ice thicknesses worldwide stem from this method. Apart from data from upward-looking sonar (and recently from satellite altimetry; see Sections 3.2.8.1 and 3.2.8.4), data sets from drill-hole measurements are probably still the most extensive data source today. Almost all knowledge about antarctic sea ice thickness comes from drill-hole data (e.g., Wadhams et al. 1987; Lange and Eicken 1991; Worby et al. 1996), and there has been a synthesis of more than 123,000

drill-hole measurements to study sea ice variability in the Canadian Archipelago (Melling 2002).

Tips and Tricks for Mechanical Drill-Hole Measurements

- Don't forget to take a shovel if you want to remove the snow before drilling; with thick, hard snow it might be easier to measure total ice thickness without removing the snow.
- Keep drill holes clean from snow or shavings (e.g., by moving the flights up and down repeatedly to flush the hole and then wiping the ice surface clear with your shoes) as they may clog the drill hole and flights can get stuck, particularly when it is very cold.
- In thick ice with high freeboard, seeing the water level can be difficult, particularly if the hole is not clean. You can better see it with a flashlight, a little float lowered into the hole, or by lowering a metal or wooden stick into the hole – you will see the water level from where the stick has become wet.
- Have a tool for release of auger flights' push-button connectors as these can be difficult to operate in the cold when wearing gloves. A small screwdriver or pin will do, and you could tie it around your wrist to never lose it.
- Make sure couplings are tight, as well as clutches if an electric drill engine is used; many flights have been lost to the sea floor.
- Avoid bending of flights by ideally disassembling them as they are retrieved from the borehole. The guys in Figure 3.2.5c must have been insane.
- Watch your hands when touching flights and couplings with the motors attached: Serious injuries ranging from cuts to dislocated fingers have been reported. Also, watch clothing (e.g., scarfs), which can get wound up and strangle you.
- Stand on the windward side to avoid engine exhaust, and watch those drops of engine oil that can spatter you.

3.2.3 EM SOUNDING

Drill-hole measurements are so tedious and slow that very often it is desirable to use a simpler method with a better performance. In addition, the accuracy of drill-hole measurements and additional information about isostasy are often not required, or freeboard or surface elevation could be obtained from laser or DGPS surveying (see below). For these cases, the classical geophysical method of electromagnetic (EM) induction sounding provides a perfect alternative to drilling.

EM sounding has been used by geophysicists for many generations on land to study the conductivity structure of the underground. This is important for mapping of objects or geological features with distinct conductivities contrasting with

the conductivity of the background rock, for example for ore bodies, groundwater, waste deposits, or unexploded ordnance. EM instruments consist of transmitting and receiving coils of wire to generate and detect low-frequency EM fields with frequencies typically ranging between a few hundred to 100,00 or 200,000 Hz. The primary field emitted by the transmitter coil penetrates through the underground, where it induces eddy currents whose strength and phase depends on the depth and conductivities of the underground materials. These eddy currents in turn generate secondary EM fields, whose strength and phase are measured by the receiving coil. From these measurements the conductivity structure or layering of the underground can be derived.

Since the mid-1980s, this method has been applied to sea ice (Kovacs et al. 1987a; Kovacs and Morey 1991). The sea ice environment provides an ideal, approximately two-layer case of highly resistive ice over infinitely deep, conductive seawater. Therefore, the primary EM field penetrates the ice almost unaffectedly into the water, where induction takes place only in a relatively thin layer under the ice, because the saline, conductive water prevents deeper penetration of the fields (Figure 3.2.8; see also animation on accompanying DVD). Strength and phase of the resulting secondary field are therefore closely related to the distance between the instrument containing the transmitting and receiving coils, and the ice-water

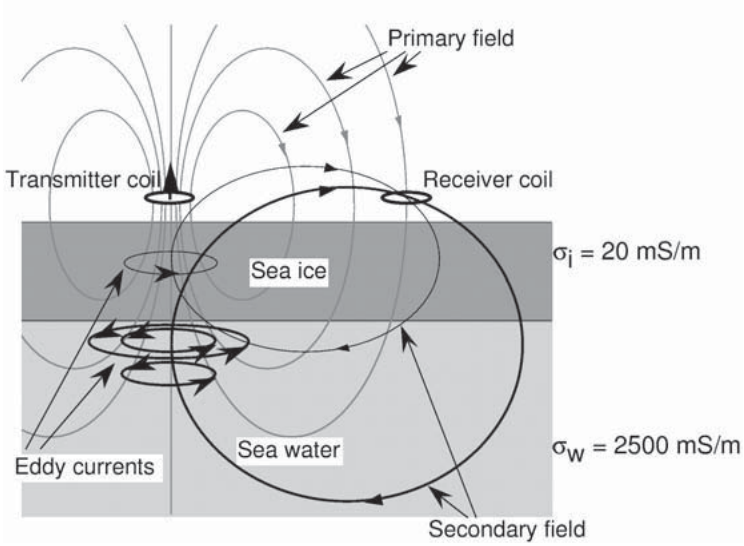

Figure 3.2.8. Principle of EM induction measurement of sea ice thickness. A primary field generated by a transmitter coil induces eddy currents primarily in the conductive water under the ice, which results in the generation of a secondary EM field, whose strength and phase are measured by a receiving coil. Strength and phase of the secondary field depend on the distance between the coils and water, which relates to ice thickness. Note that the sketch shows coils in vertical dipole configuration, which is typically not used for ground-based surveys.

interface. If the instrument rests on the ice surface, this distance corresponds to the ice thickness. However, if the instrument rests on the snow surface, the measured thickness represents total, snow-plus-ice thickness.

For many applications, total thickness is a sufficient observable, as the snow is generally much thinner than the ice. In summer in the Arctic, snow normally melts completely, such that the measured EM thickness corresponds to the ice-only thickness. However, given the importance of the snow cover as an independent climate variable and for ice thermodynamics, it is often desirable to perform additional snow thickness measurements along the same profiles, or statistically in the same region. This is also required if comparing measurements from different years to separate changes of ice thickness from changes of snow thickness.

Strength and phase of the secondary field depend not only on ice thickness and water and ice conductivity, but also on the instrument configuration, that is, the spacing between transmitting and receiving coils and the frequency of the transmitted EM field. The most commonly used EM instrument today for sea ice thickness measurements is a Geonics EM31, which has a coil spacing of 3.66 m and operates with a signal frequency of 9.8 kHz. All equations and figures following in this section refer to this instrument configuration. The instrument yields a reading of apparent conductivity σ_a in units of millisiemens per meter (mS/m), which is computed from the imaginary or quadrature component of the measured secondary EM field (McNeill 1980).

Transmitting and receiving coils of an EM instrument form magnetic dipoles. The geometry of the intersection of the primary and secondary field with the ice-water interface and the resulting field strengths differ for vertical and horizontal dipoles. The relationship between the measured secondary EM field and ice thickness differs accordingly for surveys in vertical or horizontal dipole modes (VDM or HDM), which are performed with horizontal or vertical coplanar coils (HCP or VCP), respectively. The sketch in Figure 3.2.8 illustrates horizontal coplanar coils operated in VDM. Figure 3.2.9 shows the relationship between the EM signal in VDM and HDM (expressed as apparent conductivity σ_a) and ice thickness. Note that the VDM response is arbitrary, as for typical seawater conductivities it drops off for both thinner and thicker ice from a maximum of 412 mS/m at a thickness of 0.9 m. It should only be used if it is clear that only thicknesses smaller or larger than 0.9 m are present along the profile. Therefore, the instrument is mostly operated in HDM mode, which also has a slightly smaller footprint (Kovacs and Morey 1991), the area in which most of the eddy currents are induced and over which the thickness retrieval is averaged (see below).

The relationship between the EM signal (expressed either as a relative field strength Z, in parts-per-million (ppm) of the primary field, or as apparent underground conductivity σ_a (McNeill 1980)) and ice thickness can be derived theoretically for given conductivities of the ice and water, according to:

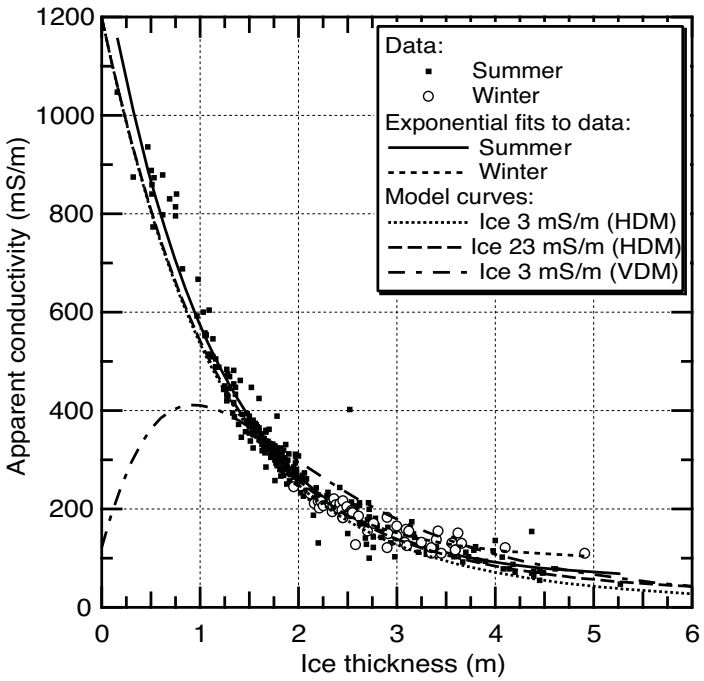

Figure 3.2.9. Measured apparent conductivity versus ice thickness for two winter and summer data sets and their exponential fits (Equations 3.2.3a,b; from Haas et al. 1997). Also plotted are three two-layer 1-D model curves for ice floating on water with a conductivity of 2600 mS/m. Ice conductivities of 3 and 23 mS/m have been assumed, and curves are shown for both, HDM and VDM.

$$Z = -r^3 \int_0^\infty r_{TE}\, e^{-2\lambda h} \lambda^2 J_0(\lambda r)\mathrm{d}\lambda \quad \text{(Equation 3.2.2)},$$

with r being the coil separation, h the receiver and transmitter height above ground, λ the wave number, and r_{TE} a recursively determined transverse electric (TE) mode reflection coefficient resulting from the electromagnetic properties of the underground. The underground is assumed as a one-dimensional model of horizontal layers with infinite lateral extent. Equation 3.2.2 is a so-called Hankel transform with a Bessel function of the first kind of order zero (J_0), which can only be solved numerically.

However, relationships between EM signal and ice thickness can also be determined empirically by comparisons between EM and drill-hole measurements as shown in Figure 3.2.9 for the EM31. It can be seen that in HDM σ_a decreases negative-exponentially with increasing ice thickness, and agrees very well with model results. Least-square fitting of a negative exponential equation can yield the desired transformation equation for deriving ice thickness z_i from measurements of σ_a. In the example of Figure 3.2.9, the fitted equations were:

$$\sigma_{a_w} = 95.8 + 1095.5 \times \exp(-0.995 \times z_{i_w}) \quad \text{(Equation 3.2.3a),}$$

and

$$\sigma_{a_s} = 57.2 + 1270.9 \times \exp(-0.900 \times z_{i_s}) \quad \text{(Equation 3.2.3b),}$$

for measurements under winter and summer conditions (sub-indices w and s, respectively; Haas et al. 1997). Inversion yields

$$z_{i_w} = 7.03 - \ln(\sigma_{a_w} - 95.8)/0.995 \quad \text{(Equation 3.2.4a),}$$

$$z_{i_s} = 7.94 - \ln(\sigma_{a_s} - 57.2)/0.900 \quad \text{(Equation 3.2.4b),}$$

for ice thickness.

Figure 3.2.9 and Equations 3.2.3 and 3.2.4 show that the performance of EM measurements under summer and winter conditions is equally good. In fact, under summer conditions the ice is warmer and more porous than in winter, but the salinity of the brine is strongly reduced. Therefore, the overall conductivity of the ice changes only slightly. From numerous ice core analyses, Haas et al. (1997) have shown that the ice conductivity varies only between 3 and 23 mS/m between winter and summer. Model curves in Figure 3.2.9 are in very good agreement. Similarly, melt ponds are mostly composed of fresh meltwater, and have a minor effect on the validity of the transformation Equations 3.2.3 and 3.2.4 (Haas et al. 1997; Eicken et al. 2001).

However, it should be noted that the equations given above are only valid for the ranges of water and ice conductivities of 2600 mS/m and 3–23 mS/m given in the caption of Figure 3.2.9. The EM response is particularly sensitive to changes in water conductivity of a few 100 mS/m, which implies that different equations have to be derived, for example, for brackish water in the Baltic or Caspian seas.

The agreement between ground-based EM and drill-hole measurements lies generally within 5 to 10 percent both in winter and summer (Haas et al. 1997). The exponential fits in Figure 3.2.9 explain 91 percent (winter) and 98 percent (summer) of the observed variability indicated by the scatter of individual measurements. The negative-exponential decline of the EM response with ice thickness implies also that with greater ice thickness small thickness variations do not cause strong signal changes, and therefore cannot be detected. In HDM, thickness changes of 0.1 m can typically be detected with the EM31 with ice thicknesses of up to 5 m. The sensitivity is slightly better in VDM, which could be well used over thick ice.

The accuracy of EM measurements and agreement with drill-hole measurements is reduced by the footprint of the EM method, which is the area under the instrument over which ice thickness is averaged. Due to the lateral extent of the

eddy currents, the resulting secondary field is induced over the area of the eddy currents. A general definition of the footprint size is the area within which 90 percent of the secondary field is induced (Liu and Becker 1990; Kovacs et al. 1995; Reid et al. 2006). The footprint implies that in general no perfect agreement between drill-hole measurements, which only yield ice thickness within a few centimeters of the drill hole, and EM sounding can be achieved if ice thickness varies laterally. While this variation is naturally small over level ice, it is large over rough, deformed ice and pressure ridges. Consequently, the maximum thickness of pressure ridges is generally underestimated because the water adjacent to the keels contributes to the EM signal and increases it (Figure 3.2.7). In contrast, on ridge flanks, ice thickness can be overestimated because the adjacent keel can lead to reduced induction of eddy currents. Overall, experience shows that maximum ridge thicknesses can be underestimated by as much as 50 percent, while the mean cross-sectional ice thickness across ridges agrees within 10 percent of drill-hole measurements (Haas et al. 1997; Haas and Jochmann 2003).

Apart from its efficiency and accuracy, the advantage of EM ice thickness measurements is that they are nondestructive and do not require any mechanical contact with the ice or snow. Nondestructive measurements are required in situations where drill holes could disturb the hydrostatic equilibrium and therefore the thermodynamic balance in longer-term studies of ice thickness change. This is relevant where negative freeboard due to heavy snow load could cause flooding after drilling (Haas et al. 2008c), or when drill holes could form artificial drainage channels during the melt season (Eicken et al. 2001). The contact-free nature of EM measurements means that an EM instrument could be deployed in a sledge or kayak to allow easy towing (e.g., by a snowmachine) and protection over various surfaces including melt ponds. However, it also allows for the deployment of EM instruments from platforms above the ice, for example from icebreakers, helicopters, or lighthouses (see Section 3.2.9 for examples), or from more advanced platforms like fixed-wing airplanes, airships, or hovercrafts.

Tips and Tricks for Ground-Based EM Measurements

- Some drill-hole measurements should always be performed at EM measurement sites to confirm the validity and accuracy of the transformation equation (according to Figure 3.2.9 and Equations 3.2.3 and 3.2.4) and to obtain a seawater sample for measurements of water conductivity, if unknown.
- Most EM instruments should be used in horizontal dipole mode to avoid ambiguities in the EM response. The EM31 operates in VDM by default. However, it can be easily operated in HDM when turned 90 degrees around its long axis, such that the instrument lies on its side and the display shows sideways.

- Geonics also provides an EM31 ICE instrument, which is supposed to be configured in HDM by default, and includes an ice thickness module that displays readings of ice thickness based on similar transformations as those in Equation 3.2.4. However, the module can only be calibrated for water conductivities between 2,000 and 3,000 mS/m.
- Use a sledge for easy pulling of instruments by snowmachines or while walking. Use a kayak for better protection and profiling over melt ponds.
- Use a data logger for continuous (analogue or digital) recording along extended profiles. Ideally, with every EM measurement the data logger should also record synchronous GPS positions to allow for later geocoding of measurements and derivation of an equidistant data set, which is required for calculation of ice thickness statistics independent of variations of ice drift or survey speed.
- Snow thickness is important! The only current operational method is using a meter stick (see Figure 3.2.3, Section 3.2.2, and Chapter 3.1). In this case, care should be taken to accurately coregister snow thickness and EM measurements, which is difficult with a data logger. Ideally, two people can efficiently read snow thickness and EM response at every measurement location and note them by writing into a notebook.
- Freeboard or surface elevation can be measured along the EM profile by means of laser or differential GPS surveying (Sections 3.2.5 and 3.2.6) to allow studies of isostasy or ice density. Obtaining a coincident data set at the same measurement locations of the EM measurements requires careful logging and/or documentation of every individual measurement.
- Use an external battery for the EM instrument to extend its longevity under cold conditions.
- Make sure batteries are equally charged! In most EM instruments, the accuracy and stability of the EM response depends critically on two equal voltages, typically +6 VDC and –6 VDC. With the EM31, voltages down to ± 4.8 VDC are acceptable.

3.2.4 GROUND-PENETRATING RADAR (GPR)

In a classical, geophysical sense, another type of EM measurement for snow and ice thickness is radio echo sounding (RES), also called ground-penetrating radar (GPR). GPR measurements employ high-frequency EM waves ranging between a few hundred megahertz to a few gigahertz. On land, GPR is successfully used in environmental and engineering geophysics to determine the thickness of thin layers (e.g., of soils, pavements, landfills, or aquifers). The method is based on measurements of the travel time of radar pulses, which travel from the transmitting antenna to an interface, where they are reflected and detected by a receiving antenna. The distance d to the reflecting interface is obtained from $d = c\ t/2$, with radar wave

propagation speed c (2.998 10^8 m/s in air) and ("two-way") travel time t between antennae and the reflecting interface and back.

According to general principles, sea ice and snow thickness measurements could provide ideal applications for GPR measurements. However, there are only very few examples published in the literature where this has been successfully achieved (e.g., Kovacs and Morey 1986; Sun et al. 2003; Otto 2004).

The problems of applying GPR to sea ice thickness measurements are manifold. Compared to other thin layers commonly surveyed in engineering geophysics, ice and snow thicknesses—typically ranging from 1 to 3 m, and 0.1 to 0.8 m, respectively—are often too thin to be accurately measured. Resolving these thicknesses requires minimum radar wavelengths between 0.4 and 12 m, corresponding to four times the layer thickness. For radar propagation speeds of approximately 0.22 m/ns in snow and 0.16 m/ns in sea ice, this results in minimum radar frequencies of 550 MHz for snow and 13 MHz for ice. For improved resolution of and distinction between the reflection from internal layers and the ice-water interface, higher frequencies are used, typically between 250 MHz and 1 GHz.

Radar reflections are caused primarily at interfaces with contrasting dielectric properties, like at the snow-ice and ice-water interfaces. The radar wave propagation velocity $v = c/\sqrt{\varepsilon_r}$ is also dependent on the dielectric constant ε_r of ice, snow, and brine. The dielectric constant of sea ice is strongly dependent on the amount and distribution of brine within the ice matrix (Stogryn and Desargant 1985; Kovacs et al. 1987b). Therefore, the propagation speed varies in dependence of ice salinity and temperature. In addition, brine inclusions themselves form small scatterers for the radar waves, leading to internal reflections and low signal-to-noise ratios. Internal scattering and absorption ("loss") are particularly strong in saline first-year ice and in warm and wet ice during the ablation season.

Figure 3.2.10 shows an example of a multiyear profile, where a good reflection from the ice underside was received (Otto 2004). The bottom panel of the figure shows a comparison of ice and snow thicknesses derived from the radar reflections with results from EM induction and drill-hole measurements. In general, a nice agreement between methods to within 0.1 to 0.2 m is visible.

The example shows that radar measurements of snow and ice thickness are generally possible, at least over cold multiyear ice. However, the radargram also reveals some general problems with varying bottom reflection amplitudes, blurring of reflections, and loss of trace-to-trace correlation, particularly in zones of rougher ice. These signal characteristics prevent easy and automatic extraction of radar two-way travel times to the reflecting interfaces, which makes processing of the radar data very labor-intensive and difficult, and which degrades their accuracy. In addition, knowledge of radar propagation speed is required to convert travel times into ice and snow thickness. These can vary by more than 0.03 m/ns, resulting in a thickness uncertainty of a few decimeters.

The blurred reflections from the undersides of both snow and ice over rougher

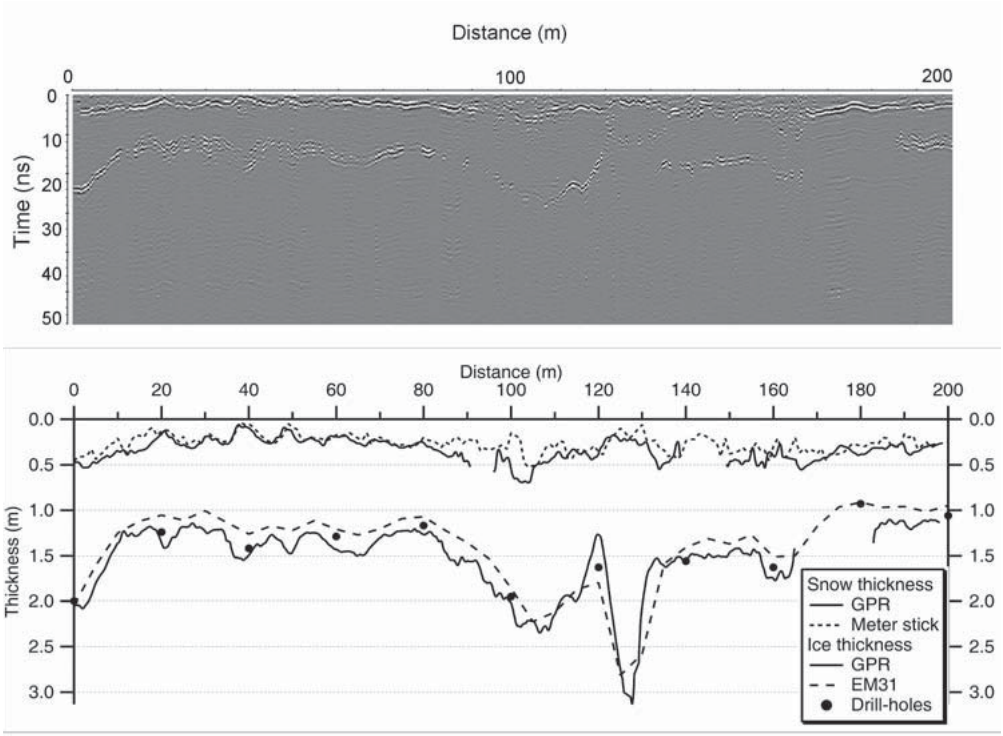

Figure 3.2.10. Top: Radargram of a 200 m long profile in the Barents Sea, obtained with a 800 MHz antenna on 1.2 m thick, cold multiyear ice, covered by 0.2 to 0.3 m of snow. **Bottom:** Comparison of radar-derived ice and snow thicknesses with results from EM sounding and drill-hole/meter-stick measurements. Ice and snow thickness was calculated using radar propagation velocities of v_{ice} = 0.158 m/ns and v_{snow} = 0.218 m/ns, respectively (Figures modified from Otto 2004).

zones are partially a result of reduced coherence of the reflected signal due to the presence of many scatterers in the radar footprint with variable distances to the antennae. This problem, and issues related to energy dispersion, become more important if radar measurements were performed from above the ice (e.g., from an icebreaker or helicopter).

However, it could be expected that many of the problems can be overcome in the future with improved instrumentation. One such example is the use of wide-band, continuous-wave, frequency-modulated (CWFM) radars, which have better penetration, resolution, and signal-to-noise characteristics than conventional systems. The potential of this technology for snow and ice thickness measurements has been demonstrated by Kanagaratnam et al. (2007) and Holt et al. (2008).

3.2.5 LASER SURVEYING OF THE GEOMETRIC SEA ICE ROUGHNESS

The small-scale variability of the thickness of sea ice implies a considerable surface roughness. Sea ice is rough on many scales from millimeters to tens of meters.

Centimeter-scale roughness is important for sea ice microwave properties and is sometimes referred to as "radar roughness." Here and in the subsequent sections, we focus on the "geometric roughness" of the ice, which relates to features with dimensions of decimeters and greater. Geometric roughness is generally caused by features like pressure ridges, rubble, rafts, snowdrifts, and sastrugis, or melt ponds. Geometric roughness is important because it can possibly be used as a proxy for ice thickness; it strongly modifies the surface drag of the ice, and therefore the interaction between ice and atmosphere; it acts as obstacle for the redistribution of snow; and it determines the hydrological drainage network during the melt season. A measure of surface roughness is the root-mean-square (rms) roughness, which is the standard deviation of a roughness or surface elevation profile. Pressure ridge distributions—that is, the number, height, and spacing of ridges in short intervals along a profile or within a given area—are also used to quantify surface roughness. The derivation of ice thickness from measurements of surface elevation is discussed further in Section 3.2.8.4.

Many geodetic surveying methods are available for observations of the surface morphology and roughness. A fast and accurate alternative to standard theodolite measurements is surveying with a rotating, self-leveling laser (Figure 3.2.11). This is a horizontally rotating laser whose laser beam forms a horizontal reference plane.

Figure 3.2.11. Rotating laser on a tripod placed on a small ridge. Two people with the laser detector attached to a range pole can be seen in the far back.

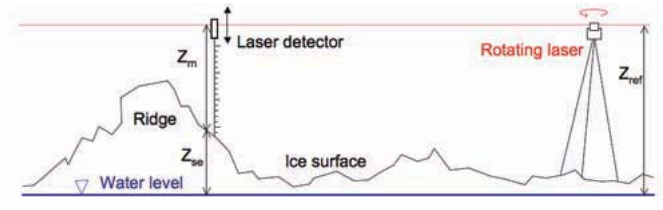

Figure 3.2.12. Illustration of laser surveying of ice surface elevation Z_{se} by means of a rotating laser forming a reference plane at height Z_{ref} above the water level. The height Z_m of the reference plane above the snow surface is measured with a laser detector, usually mounted to a telescopic range pole.

The height Z_m of this reference plane above the ice surface can be measured with a laser detector (Figures 3.2.3 and 3.2.12), which acoustically or optically indicates when it is detecting laser light and is therefore exactly within the reference plane. The laser detector can be mounted onto a telescopic range pole for easy height measurements. The height Z_{ref} of the reference plane above the water level has to be measured once at the beginning of the survey (e.g., over a drill hole or crack in the ice). Surface elevation results as $Z_{se} = Z_{ref} - Z_m$ (Figure 3.2.12).

A typical surface elevation profile surveyed by laser leveling is included in Figure 3.2.7, where it is also compared with the surface elevation from drilling. A good agreement between both measurements can be seen. The accuracy of laser surveying, which is mainly determined by the narrowness, stability, and horizontal alignment of the laser beam and by the sensitivity of the detector, ranges between 0.5 and 1.0 cm. Significant disagreement with drill-hole measurements results mainly from slight variations in the actual sampling sites in rough ice or over a rough snow surface. This can be seen in a few locations in Figure 3.2.7 where the drill hole has been drilled in the lowest locations (e.g., next to a rafted ice block), while the laser measurement has been performed on the crest of the ice block, with only a lateral distance of 0.1 to 0.2 m between them.

Note that either the snow surface elevation or ice surface elevation (freeboard) can be measured, and that both can be derived from each other if snow thickness is known. However, measuring the snow surface elevation is generally easier, although over soft snow precautions have to be taken to avoid the laser detector range pole from penetrating into and below the snow surface.

Efficient surveying requires at least two people, one to perform the measurement and one to take notes. However, there are also range poles available with attached data loggers, which allow one person to perform the measurements alone.

Tips and Tricks for Laser Surveying of the Geometric Surface Roughness

- Place the laser tripod firmly onto the ice surface, as later settling of the snow or movements of individual legs due to melt could result in small laser movements with consequent interruption of its rotation and the possible loss of the original geometry and reference level.
- Place the laser in the center of the profile, such that its range (approximately 200 m for most lasers under clear weather conditions) can be fully utilized on both sides of the laser location.
- Place the laser tripod on a high point along the profile and raise the laser just high enough so that it is above the height of the highest ice feature along the profile plus the minimum length of the range pole.
- Take careful notes of measurement location for later merging with other data sets, for example from EM sounding.
- Fog, rain, or snow can scatter the laser beam and result in a loss of the signal at the detector. The detector can be irritated by direct incident sunlight and might have to be shadowed.
- Avoid penetration of the range pole into the snow if snow surface elevation is to be measured. Over soft snow this can be tedious, but the range pole can be placed on a foot, for example, which is stamped into the snow with its upper edge located at the same height as the snow surface.

3.2.6 DGPS SURVEYING OF SURFACE ELEVATION

The collection of differential global positioning system (DPGS) data is another method for obtaining measurements of freeboard, surface morphology, and roughness, with accuracies achieved at ±0.01 m. Eventually, these measurements can also be used to derive ice thickness (see Section 3.2.8.4 for a detailed discussion of potentials and constraints). DGPS methods improve upon the accuracy of standard GPS measurements through the use of phase information of the GPS signals received by two GPS receivers. One receiver is used along the profile to collect the height measurement (the roving receiver) and the other is used as a stationary reference (or base) receiver positioned at a known point. Figure 3.2.13 shows an example of what this setup might look like in the field. Using simultaneously collected data from the base receiver, the solution obtained for the position of the roving receiver is corrected for various errors, including those associated with satellite clock and orbital drift and regional ionospheric conditions. The accuracy of DGPS is improved the smaller the baseline distance is between the two receivers. This is because the corrections applied to the roving receiver's solution generally rely on the two receivers using the same satellite constellation and also because a more accurate calculation is made when these shared satellites are located high above the horizon (i.e., the signal path length between satellite and receiver is minimized).

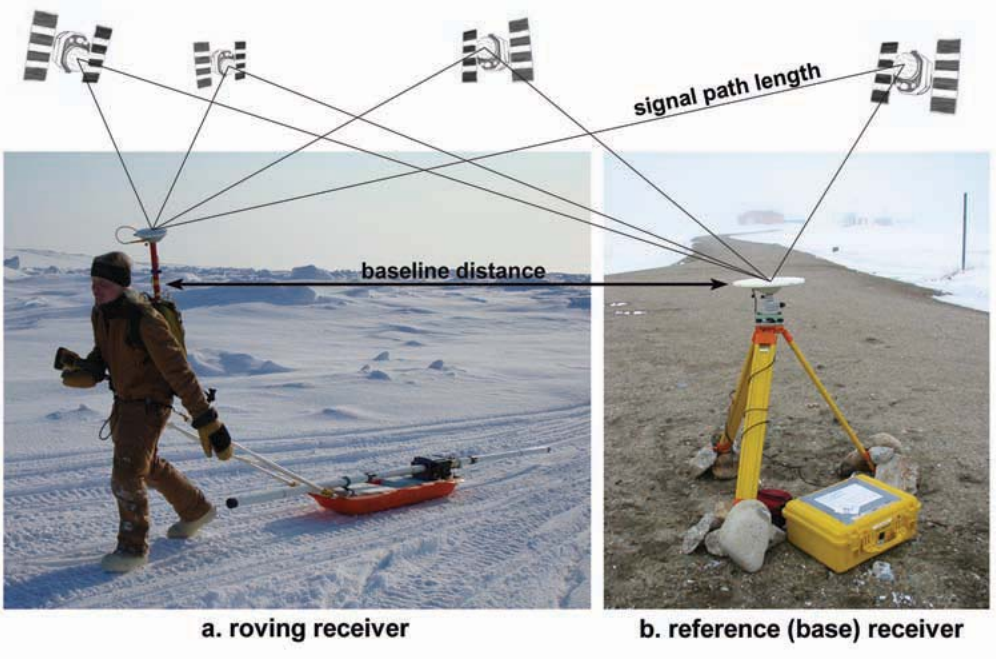

Figure 3.2.13. Example DGPS set-up for measuring the surface roughness of landfast sea ice. The roving receiver in Figure 3.2.13a is mounted on a backpack. An EM-31 is in the sled being pulled. The reference, or base, receiver is shown in Figure 3.2.b. The straight line distance between the two receivers is referred to as the baseline distance.

DGPS positioning can be obtained either through postprocessing of data or in real time using a radio-transmitted correction from the base to the roving receiver. In the latter case, the survey depends on the two receivers maintaining radio contact, which can be difficult when surface topography is highly variable.

The survey style should be chosen based on the desired spatial coverage, sampling frequency, time available for the survey, and desired level of accuracy. Continuous surveys, set to make observations at either selectable time or distance intervals, are typically employed when sampling over large distances, field time is limited, or when the roving receiver setup is not conducive to point-based measurements, such as when attached to a moving vehicle (e.g., helicopter, snowmachine, sled). The time stamp in continuous DGPS data is typically used to coregister the measurements with other forms of simultaneously collected data sets, such as EM-derived measurements of ice thickness.

In contrast to continuous surveys, point measurement surveys rely on the occupation of specific points of interest for a set period of time in order to obtain greater accuracy. An additional advantage to point measurements is that the data is easily labeled and assigned to features of interest. For example, if one wished to measure surface elevation along a 100 m transect at 5 m intervals and merge this data set with ice thickness measurements made at the same spacing, a point survey would be preferred (cf. Figure 3.2.7). A disadvantage to this method is that it is time-intensive compared to continuous surveys.

Major advantages of DGPS surveying compared with laser surveying are its principally unlimited range, allowing one to measure long profiles without the requirement to relocate any instruments like the laser, and its additional provision of very accurate location information, which is required to geolocate the height measurements and eventual additional observations. Figure 3.2.7 shows a typical surface elevation profile obtained by DGPS surveying, and compares it with the surface elevation from drilling and laser surveying. Again, a good agreement between both measurements can be seen. As discussed above with respect to laser surveying, disagreement with drill-hole measurements results mainly from slight variations in the actual sampling sites in rough ice or over a rough snow surface.

DGPS surveys for ice morphology and roughness can be performed in a number of different setups. The most common are with the receiving unit on a pole, tripod, backpack (see Figure 3.2.13), or vehicle. In any case, the following should always be considered when performing a survey:

Tips and Tricks for DGPS Surveying of the Geometric Surface Roughness

- Plan the survey for a time of day when the number of the satellites in the constellation overhead is relatively great.
- Ensure setup of the receivers allows for unobstructed views of the sky at all times.
- Keep notes of the type of GPS receivers and antennas used for the survey, as this information is very important during data processing.
- Make detailed notes on receiver settings, such as observation frequency and those settings specific to how the receiver chooses which satellites to use (e.g., antenna mask, position dilution of precision [PDOP], etc.).
- Always remember to measure antenna height above the surface of interest (e.g., the surface of the ice) before the survey, and also afterwards to ensure the antenna height was not altered during the survey.
- Note that DGPS-derived surface elevation measurements refer to a global ellipsoidal geodetic model. This can locally deviate from the geoid (i.e., the true height of the water surface) by several tens of meters. Therefore, the difference between the geoid height and ellipsoidal height has to be compensated before "true" surface heights above the local water level can be obtained. If possible, a hole should be drilled into the ice, either immediately before or after the survey, to make a point observation of the surface elevation of the water. This measurement allows for the observations of ellipsoidal ice surface elevation to be easily converted to measurements of freeboard, which will equal the surface elevation minus the water elevation. Note that ocean tides cause a slow drift in the surface elevation measurements, which can be corrected by two reference measurements

over water before and after the survey. Otherwise, all DGPS measurements can be referred relative to some local surface elevation of unknown absolute height.

- Surveying an ice surface with a snow cover requires special consideration. For point surveys, it may be easiest to shovel the snow and measure directly from the ice surface. When continuously surveying from a moving vehicle, such as a sled or snowmachine, one may only be concerned with average snow thickness. In this case, estimating the vehicle's depression into the snow cover may help correct for a more representative survey of the ice surface. However, DGPS can also be very useful in measuring the surface roughness of the snow cover as well.

3.2.7 ICE MASS BALANCE BUOYS AND HOT-WIRE THICKNESS GAUGES

All methods presented so far can be used to obtain long profiles of ice thickness data within a relatively short time. However, it is difficult to perform measurements over a longer time period to study temporal changes, as field personnel has to be present throughout. In contrast, automatic measurement stations can be deployed on the ice to provide long-term data of ice thickness changes at one location, either on fast ice or on a drifting ice floe, in which case ice thickness changes are observed along the drift track of the floe. These automatic stations are commonly called ice mass balance buoys (IMBs) (Richter-Menge et al. 2006). A more comprehensive discussion on how to operate these buoys automatically and transmit their data via satellite is given in Chapter 3.13.

A typical IMB consists of acoustic range finder sounders to measure snow accumulation and ablation and ice bottom growth and melt, and of a thermistor string to observe internal ice temperature profiles (Richter-Menge et al. 2006). The latter normally extents into the water and therefore provides additional measurements of water temperature, while an additional air temperature sensor provides above-surface temperature data. Relative changes of surface elevation and draft can be easily calculated from changes of the acoustically derived distance to these surfaces. Reductions in measured distances indicate snow accumulation and bottom growth, while increased distances are due to surface and bottom melt. The accuracy of these measurements is typically better than 1 cm. Note that absolute changes of freeboard, surface elevation, and draft with respect to the water level cannot easily be determined. Freeboard changes can only be determined if an additional pressure sensor is used in the water. All measurements together not only allow thickness change observations, but can also be used to address the role of various atmospheric and oceanic boundary conditions for these changes.

The combination of surface and bottom sounding with air, ice, and water temperature measurements is a powerful means to study the thermodynamic

development of the ice. However, as IMBs obtain data only at one location, they cannot yield any information on dynamic ice thickness changes due to rafting and ridging, and therefore cannot access the complete ice mass balance on a floe or at the regional scale. In addition, results are strongly dependent on local conditions, for example, whether the sensors are located on ponded or unponded ice, or if a snowdrift develops under the sounders. The buoy itself might modify the sea ice mass balance through preferential melting by absorption of radiation during the summer, or by disturbing airflow and therefore the wind-induced redistribution of snow.

Longer-term changes of draft and surface elevation can also be measured by means of so-called thickness gauges. These consist of an ablation stake and a hot-wire thickness gauge, and their design and operation is described in great detail by Mahoney and Gearheard (2008). Extensive measurements were made, for example by Perovich et al. (2003) during the Arctic Surface Heat Budget of the Arctic (SHEBA) drifting station. A long, wooden stake painted white and marked with metric tape can serve as an ablation stake, frozen into a deep drill hole that does not extend through the ice. The hole should be deep enough to prevent melting out of the stake during the summer. Surface elevation can be measured off the stake with an accuracy of 0.5 cm by noting the intersection of the stake with the snow surface. A hot-wire thickness gauge consists of a stainless-steel wire with a steel rod attached as a crossbar on the bottom end and a wooden handle on the top end. It is installed adjacent to the ablation stake. To make a measurement, the stainless-steel wire is hooked to a generator that is also connected to a copper wire grounded in the ocean. The electrical resistance of the stainless-steel wire melts it free, and the handle can be pulled upward until the steel rod hits the bottom of the ice. Then, the handle position is read off the ablation stake to give the position of the ice bottom. Instead of a stainless steel wire and generator, electric heating cables as used for example in pipe antifreeze applications can be frozen into the ice. These cables heat when connected to a 12V or 24V battery, for example. Uncertainties of stake and gauge readings are typically less than 0.5 cm.

Operation of thickness gauges is almost similar to performing repeated drill-hole measurements at the same location. However, the mechanical and thermal destruction and disturbance of the original ice and snow layers are reduced to a minimum. The holes resulting from melting the wires is very narrow, and refreezes quickly after the power source is disconnected.

3.2.8 ADVANCED METHODS

This section presents more advanced techniques for sea ice thickness measurements. Although the methodological principles are generally simple, major challenges exist in the technical realization of these concepts and to meet the required accuracies. In addition, all sensors over or under the ice have to be deployed by

some means of transport and logistics, usually ships, aircraft, submarines, or satellites. This involves significant cost, prohibiting broad and flexible application. Even though today the operation of satellites is taken for granted by many, it should be noted that the ground segment (i.e., satellite control and the reception, processing, and distribution of data) requires significant computational resources and expertise. In addition, mission planning and extension is often politically driven, and may prevent the acquisition of long-term, systematic data sets. However, there are many efforts underway to improve this situation. In addition, initiatives are progressing to at least make the high-level, final thickness data sets available to a broad public in uniform formats, such that data sets from individual methods can be merged to yield long and spatially dense records of general ice thickness conditions in the polar oceans.

3.2.8.1 Upward-Looking Sonar (ULS) Profiling of Ice Draft

Due to the density of sea ice of approximately 920 kg/m^3 (Chapter 3.3), the draft of freely floating sea ice is approximately 9/10 of its thickness if the snow cover is neglected. This suggests that draft can be used as an accurate proxy for ice thickness. Indeed, most of the ice thickness data gathered to date have been derived from measurements of ice draft performed by upward-looking, range-finding sonar (ULS) or ice-profiling sonar (IPS). These have been operated on both submarines (e.g., Bourke and Garret 1987; Rothrock et al. 1999; Wadhams and Davis 2000; Rothrock et al. 2008) and oceanographic subsea moorings (e.g., Vinje et al. 1998; Strass and Fahrbach 1998; Melling et al. 2005), respectively.

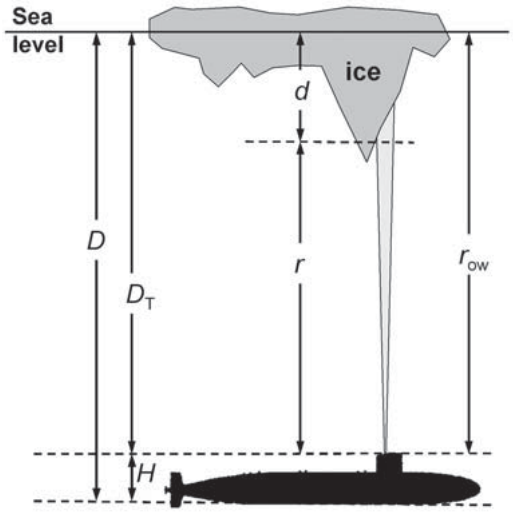

Figure 3.2.14. Schematic drawing showing how ice draft d measurements are obtained by ULS from a submarine (from Rothrock and Wensnahan 2007). The depth of the submarine *D* is determined by a sensor that measures pressure *p* and is calculated as $D = (p - pa)/((\text{water density}) \times g)$, where *g* is the acceleration of gravity and pa is sea level pressure. The height *H* is the vertical distance from the pressure sensor to the sonar transducer, which is mounted on top of the submarine at a depth D_T. The range *r* is the distance to the ice, while r_{ow} is the distance to open water, determined when the sonar passes under open water.

The measurement principle is illustrated in Figure 3.2.14 for the case of a ULS operated on a submarine. Ice draft is derived from measurements of the two-way travel time of short acoustic pulses between the sonar and the ice underside, from where they are reflected or scattered back to the sonar. The distance r between ice and sonar transducer results from $r = v\,t/2$, with two-way travel time t and sound velocity in water $v \approx 1436$ m/s. The depth D_T of the transducer below the water level is determined with a pressure sensor, and by taking into account the vertical distance H between pressure sensor and transducer. Draft d results from the difference of the depth and distance measurement: $d = D_T - r$.

Sonars used for ice draft profiling typically operate with acoustic signal frequencies of a few hundred kilohertz, corresponding to subcentimeter wavelengths. They have focused beams of 1 to 3 degrees width, limiting the sonar footprint at the ice underside to less than 10 m even for ULS depths as low as 150 m below the water level. Many sonars do not only measure travel time, but also yield an estimate of the echo amplitude, which allows retrieval of the roughness and type of the reflecting interface (e.g., open water; thin, new ice; or thick ice) (Melling 1998).

The accuracy of ULS draft measurements is affected by system precision, uncertainties in the sound velocity profiles between the transducer and ice, and weather-related variations of air pressure, which directly enter the depth measurement. For correction of sound velocity and air pressure effects it is essential that open water is repeatedly present along profiles to provide a zero-draft reference range r_{ow} to which measurements under ice can be related (Melling et al. 1995). Unfortunately, detection of open water can be very difficult when leads are narrow or when waves or swells alter the echo characteristics of the sonar signal. Some of these problems can be better addressed if high pulse repetition rates are chosen to obtain a good spatial resolution of leads, and if echo amplitude information is utilized. High pulse repetition frequencies pose a challenge for data logging and battery capacities of moored ULS operated for long periods of at least a year.

Other uncertainties of the draft measurements result from the sonar footprint (Vinje et al. 1998), which leads to systematic overestimates of ice thickness in regions of deformed ice, and from instrument tilt due to current drag on moorings or variations in submarine trim. However, detailed studies of ULS measurements show accuracies of around 0.05 m for moored instruments (Melling et al. 1995; Strass and Fahrbach 1998) and biases of +0.29 m with a standard deviation of 0.25 m for former U.S. Navy submarines (Rothrock and Wensnahan 2007).

With ULSs mounted on submarines or autonomous underwater vehicles (AUVs), long profiles can be surveyed in a very short time to provide snapshots of regional and basinwide thickness distributions. In contrast, ULSs operated on moorings can provide long time series of ice thickness change at one location. If ice drifts over the mooring, as is mostly the case, a ULS provides Eulerian information about the spatial ice thickness distribution along the trajectory of the ice. One of

the longest records has been obtained in the Beaufort Sea, and now provides a more than 12-year-long observational data set of ice thickness variability and trends for analyses of arctic climate variability (Melling et al. 2005).

Despite the great potential of submarine measurements, it should be noted that these can only be performed onboard military nuclear submarines, to which only few scientists from the USA and UK have access. Military submarine operations are usually classified, and data is only released after many years and with some geographic blurring, which does not allow any near-real-time studies. However, data from some 40 cruises between 1975 and 2000 is now publicly available at the National Snow and Ice Data Center in Boulder, Colorado, providing comprehensive data of ice thickness decline in the Arctic (http://nsidc.org/data/g01360.html). Although there were dedicated science missions onboard U.S. submarines within the Scientific Ice Experiments (SCICEX) program between 1995 and 1999, the future of that program and of the release of new data is presently uncertain. In the Southern Ocean, military and nuclear submarine operations are prohibited by the antarctic treaty. However, AUVs could potentially gather as extensive and accurate data once navigational issues are resolved to facilitate more reliable operations under ice (Dowdeswell et al. 2008).

Many difficulties exist also with the operation of moorings. Their deployment, operation, and recovery in deep or ice-covered water is very challenging and expensive, as it requires logistics support by ships, airplanes, or helicopters and potentially divers. In shallow water, there is always a risk of damage or loss of equipment due to ice scouring by ridge keels or icebergs. Iceberg collisions are common in the Southern Ocean, where tabular icebergs with drafts of several hundred meters sometimes collide with moorings. There, ULSs are normally operated in greater depths to avoid collisions with even more abundant smaller icebergs, despite consequences for the accuracy of the measurements due to greater beam divergence and sound travel distance. In almost every seasonal ice zone, moorings are sometimes damaged or removed by commercial trawl fishing.

An alternative to single-beam sonars are Acoustic Doppler Current Profilers (ADCPs) (Shcherbina et al. 2005; Bjørk et al. 2008). ADCPs are normally used to measure profiles of water current speeds by means of the Doppler shift of acoustic signals emitted at various wide angles by the ADCP and scattered back from individual water layers. However, ice draft can be estimated using the distance between the ADCP and the range cell with maximum echo intensity. The bin size of the ADCP resolution cells is typically 1 m, but it is possible to increase the resolution to about 0.1 m by fitting a Gaussian model curve to the vertical echo intensity distribution. The maximum point of the Gaussian curve can then be used to determine the distance from the instrument to the lower ice surface.

Apart from single-beam sonar profiling, multibeam sonars have also been used to obtain quantitative two-dimensional information about draft and roughness of the ice underside (e.g., Wadhams et al. 2006). These can be used from both

submarines and AUVs. Like with laser scanning (Section 3.2.8.3), two-dimensional mapping allows for observing the across-track spatial distribution of under-ice features. This reduces sampling biases in the analysis of thickness data, and can contribute to improved detection of open water. However, for distinguishing between thin ice and open water it is still required to carefully analyze echo amplitudes or the textural characteristics of the target area. Two-dimensional data is valuable for the validation of measurements with larger footprints, for example, from EM sounding and satellite remote sensing.

Due to the large draft-to-thickness ratio *R* of approximately 0.9, uncertainties in the draft profiles result only in relatively small errors in calculated ice thickness. Consequently, ice thickness is normally simply calculated from draft using a single *R* value, e.g., of 0.89 (Rothrock et al. 1999) or 0.93 (Rothrock et al. 2008), depending on whether the effect of snow is included or what snow thickness and density are being assumed. Although the uncertainty of *R* introduces uncertainties of some centimeters to a few decimeters in calculation of ice thickness, depending on actual ice and snow thicknesses, the problem is much more serious with the calculation of ice thickness from measurements of freeboard or surface elevation (Section 3.2.8.4).

3.2.8.2 Airborne EM

As mentioned in Section 3.2.3, one advantage of EM measurements is that they do not require contact with the ice, and can therefore be performed from airborne platforms. Consequently, helicopter-borne EM (HEM) surveys of sea ice thickness have been performed since the 1980s (Kovacs et al. 1987a). Similar to EM sounding in general (Section 3.2.3; see also animation on accompanying DVD), this method is principally based on the generation of a primary field and measurement of a relative secondary field strength from which the distance between the EM instrument and ice-water interface h_w is derived (Figure 3.2.15).

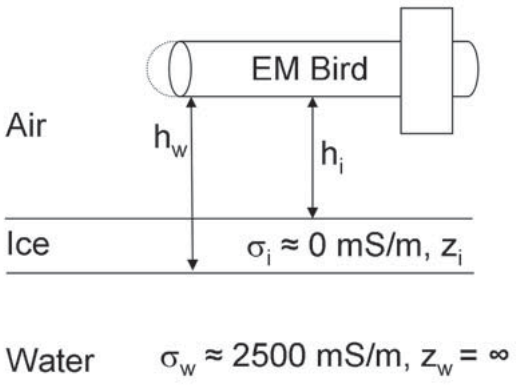

Figure 3.2.15. Principle of EM thickness sounding, using a bird with transmitter and receiver coils and a laser altimeter. Ice thickness Z_i is obtained from the difference of measurements of the bird's height above the water and ice surface, h_w and h_i, respectively. H_w is obtained with the assumption of a negligible ice conductivity σ_i, known water conductivity σ_w, and horizontal layering (Haas et al. 2008b).

Figure 3.2.16. EM bird in operation.

Normally, the transmitting and receiving coils are housed in a cylindrical shell towed by a helicopter and called an "EM-Bird" (Figures 3.2.15 and 3.2.16) (Kovacs et al. 1987a; Prinsenberg and Holladay 1993; Haas et al. 2008b). However, there are also systems where the shell is hard mounted at the nose of the helicopter (the so-called IcePic) (Prinsenberg et al. 2002), or where the coils are at the wing tips of a fixed-wing aircraft (Multala et al. 1996). In any case, as the EM system is operated at some altitude, it is required to also measure its height h_i above the ice surface, which is normally achieved with a laser altimeter. Then, ice thickness z_i results from the difference of the two distance measurements (Figure 3.2.15):

$$z_i = h_w - h_i \quad \text{(Equation 3.2.5).}$$

Here, it is important to note that this approach and equation imply that ice thickness is actually total ice thickness (i.e., ice-plus-snow thickness; cf. Figure 3.2.15). While this is not a problem during the arctic summer, when ice is usually snow-free, snow thickness at other times of the year has to be obtained by other means if ice and snow thickness are to be distinguished. A helicopter system has the advantage that snow thickness can be measured manually in situ at a few locations where the helicopter lands.

A key issue in the retrieval of ice thickness is the inversion of the electromagnetically determined field strength to ice thickness. As discussed in Section 3.2.3, this can be done by numerically inverting the solution of a forward model, either for one-dimensional (Equation 3.2.2) (Rossiter and Holladay 1994) or two-dimensional

(Liu and Becker 1990) underground models. However, those procedures require very accurate sensor calibration and the use of several frequencies to invert not only for ice thickness but also for the conductivity of the underlying seawater.

However, the inversion can also be performed more empirically by fitting an exponential function to the open-water-only response of the EM signal (Haas et al. 2008b), similar to the procedure described in Section 3.2.3 with respect to Figure 3.2.9 and Equations 3.2.3a,b. Figure 3.2.17 shows the relationship between bird height above the ice surface and measured and modeled EM responses for a flight over a typical sea ice profile. The model results have been computed using Equation 3.2.2 for open water (ice thickness of 0 m) with a seawater conductivity of 2,500 mS/m, representative of in situ salinity measurements. The model curve provides the general means of computing the height of the bird above the water surface h_w or ice from a measurement of the EM field strength at a certain height above the water. Measurements at different heights are obtained because the altitude of the helicopter and bird vary between 10 and 25 m during the flight. The data can be separated into two classes: (1) where open water measurements at different bird heights agree well with the model curves; and (2) where the presence of sea ice leads to a reduction of the measured EM signal at a given laser height (Figure 3.2.17). Therefore, the

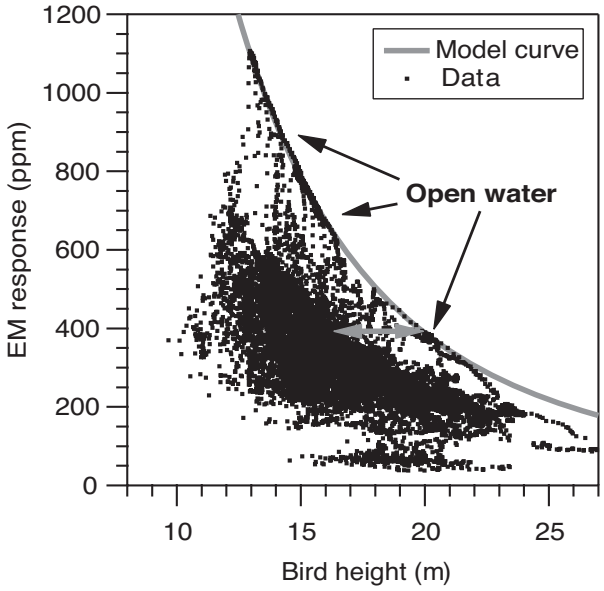

Figure 3.2.17. EM signal (Inphase component) versus bird height h_i. A model curve for open water with a conductivity of 2500 mS/m and data over a typical ice cover with some leads are shown. The horizontal arrow illustrates how ice thickness (4 m) is obtained for a single data point from the difference between h_i and the model curve h_w for a given EM field strength (Equation 3.2.5). Reprinted from the Annals of Glaciology with permission of the International Glaciological Society.

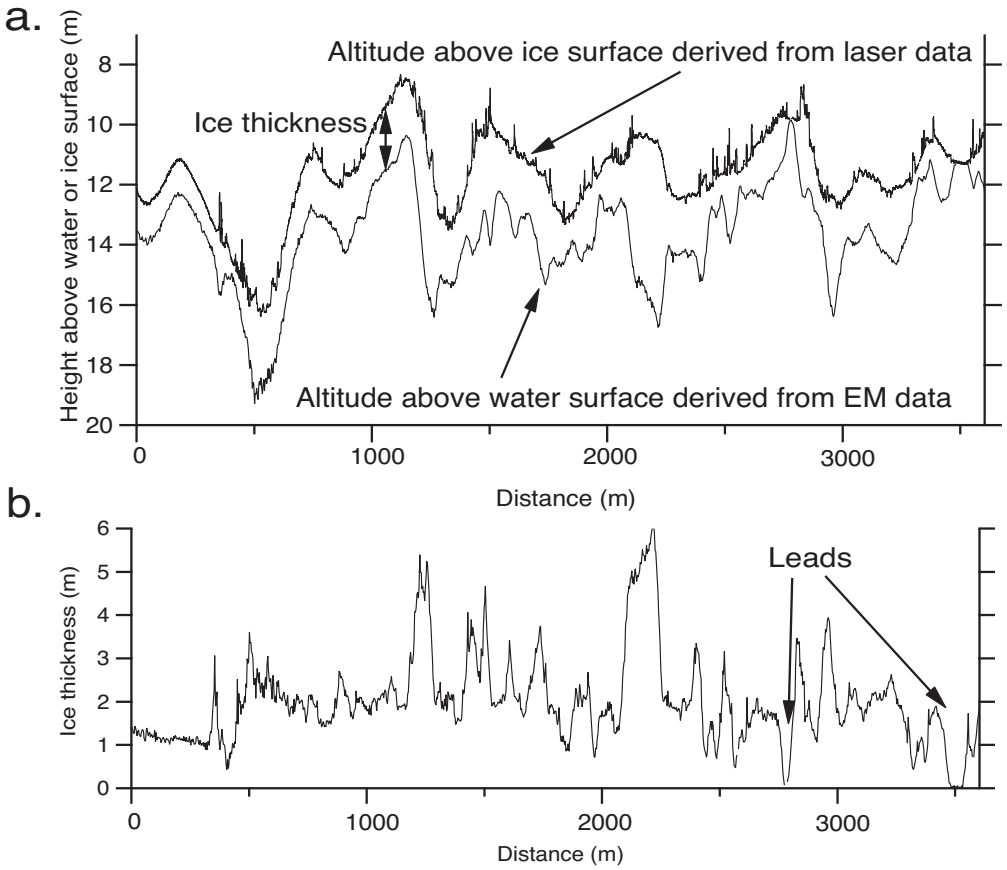

Figure 3.2.18. (a) EM and laser derived bird height above the water h_w and ice surface h_i, respectively, and **(b)** ice thickness profile resulting from subtraction of the latter from the former (Haas et al. 2008b).

scattered cloud of data points below the model curve represents measurements over ice. Ice thickness is computed by subtracting the laser height measurement over sea ice from the model curve. It can also be visually estimated from the horizontal distance between each EM measurement and the model curve (Figure 3.2.17). The thickness computation assumes a negligible sea ice conductivity of < 20 mS/m—a reasonable assumption in most cases (Haas et al. 1997; Pfaffling et al. 2007).

The advantage of this approach is that it can be performed with only one channel of EM data, and is less sensitive to inaccuracies of the instrument calibration and uncertainties in the conductivity of ice and water. Figure 3.2.18 illustrates the two steps of determining the height above the ice and water surfaces h_i and h_w, and obtaining ice thickness from the difference of these measurements. Individual ice floes with ridges, as well as thin ice on leads, can be clearly seen.

The occurrence of open water provides a convenient way to verify the calibration of the instrument. With this respect, airborne EM measurements take as much advantage of open water as all other advanced methods discussed in this chapter

(i.e., ULS and airborne laser profiling, and satellite altimetry). However, once the conductivity of the seawater is known, which can be assumed with sufficient accuracy for most regions of the Arctic and Southern oceans, the calibration of the measurements depends only on the electronic stability of the instrument components, and not on external factors like tides, currents, or sea-level pressure as with the other methods. As was shown by Haas et al. (2008b), the calibration of typical airborne EM systems is stable to within 0.1 m over a long time. Only thermal drift can be significant, but can be compensated during high-altitude flight periods.

As with ground-based EM measurements, it is important to realize that the EM response is strongly dependent on the conductivity of the underlying water. Therefore, the sensitivity and accuracy of EM ice thickness measurements decreases with decreasing salinity. However, even with salinities as low as 3 ppt as typical, for example, for the northern Baltic Sea, successful measurements have been performed (Multala et al. 1996; Haas 2004). The EM response is also strongly dependent on operating altitude: Better results are obtained for lower flying heights. Very low altitudes can be assumed with a fixed-mounted system; however, the flying speed and range are then limited (Prinsenberg et al. 2002).

The accuracy of airborne EM measurements is typically 0.1 m over level ice (Pfaffling et al. 2007; Prinsenberg et al. 2002). However, the footprint of the method is much larger than for ground measurements, and is estimated to range between 3.7 and 10 times the flying altitude for horizontal coplanar coil configurations (Kovacs et al. 1995; Reid et al. 2006). This results in stronger underestimation of maximum keel depths, although a proper validation of the accuracy of EM measurements over three-dimensionally varying natural ridges is still pending. However, the method is well capable to provide reasonable mean ice thicknesses across ridges and to compare the relative difference in abundance and thickness of ridges in different regions. This is demonstrated in Figure 3.2.19, showing a comparison of drill-hole and HEM thicknesses along a 500 m long profile. The bird altitude was 20 m, resulting in a footprint size of ~60 to 80 m. The underestimation of the ridges is very obvious. However, two parallel drill-hole profiles obtained 20 m to both sides of the plotted line, and aerial photography also

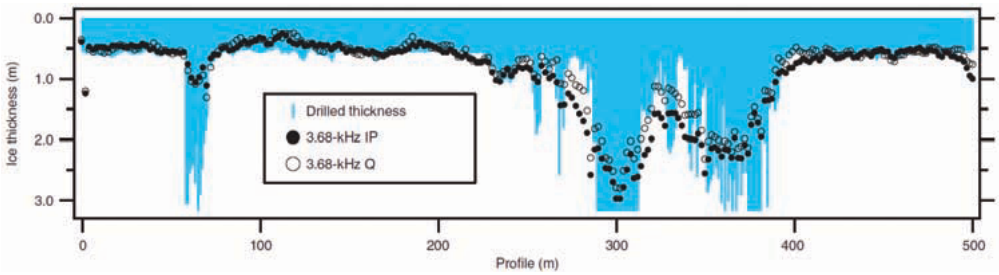

Figure 3.2.19. Comparison of drill-hole and HEM derived (In-phase IP and quadrature Q channels) ice thickness profile (Pfaffling et al. 2007). The graph does not display the maximum 5.8-m drilled ridge thickness at 305 m.

showed strong lateral inhomogeneities in the main ridge structure over the footprint area, which contributes to the disagreement visible in the one-dimensional profile in the figure.

Due to the requirements imposed by arctic logistics and by operations from small helicopters and from landing pads on icebreakers, EM birds for sea ice thickness are much smaller than instruments normally used in exploration geophysics, which provides a challenge for their signal-to-noise characteristics. Typical instruments are 3 to 5 m long and weigh 100 to 150 kg. Single and multifrequency instruments are used with typical signal frequencies between 1 and 100 kHz. Sampling rates are up to 10 Hz, corresponding to a typical point spacing of 3 to 5 m between individual measurements, depending on flying speed. The laser data are normally acquired with a higher sampling rate (e.g., 100 Hz), resulting in a relatively high-resolution profile of surface roughness (cf. Figures 3.2.19 and 3.2.21). The laser data require separate processing as described in the next section.

3.2.8.3 Airborne Laser Profiling

Due to the general isostasy of sea ice, and following the principles outlined with respect to measurements of ice draft in Section 3.2.8.1, sea ice surface elevation and freeboard can be used as a proxy for ice thickness. The thicker the ice, the higher its surface rises above the water level. In fact, with proper knowledge of the thickness of the snow cover and of the densities of ice and snow, ice thickness can be accurately calculated from surface elevation. A detailed discussion of the associated uncertainties is presented in Section 3.2.8.4. In addition, the surface profile includes information about the height and frequency of ridges and ice morphology, therefore providing information on the deformational history of the ice which can also characterize different ice regimes.

Long profiles of surface roughness and elevation can be obtained by means of airborne laser altimetry, with a vertically downward-looking laser distance meter

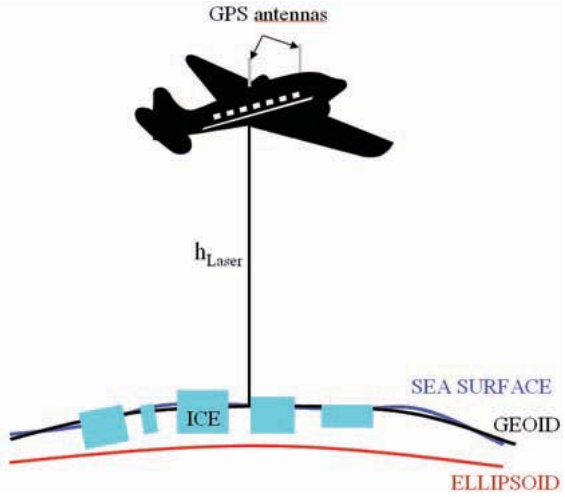

Figure 3.2.20. Principle of airborne laser altimetry (courtesy R. Forsberg). The height h_{Laser} of the aircraft above the ice and water surface is measured by means of a laser altimeter. The actual sea surface height above a reference ellipsoid is dependent on tides, geostrophic currents, and sea level pressure (dynamic sea surface topography), and varies additionally with geoid undulations due to the mass distribution within the Earths crust and upper mantle.

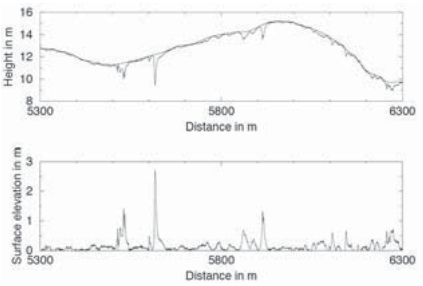

Figure 3.2.21. One-kilometer long section of a helicopter-borne laser profile. The raw data and the derived helicopter motion are shown (top) as well as the profile of surface height resulting from subtraction of the latter from the former (bottom).

operated from a helicopter or airplane (Figure 3.2.20). Such studies were performed as early as the 1960s (e.g., Mock et al. 1972). Figure 3.2.21 shows an example of a short profile thus obtained. The data are characterized by a high-frequency signal resulting from the small-scale changes of ice surface elevation including ridges, superimposed on a slowly varying signal resulting from altitude variations of the aircraft. The challenge for data processing of any kind of altimetry data is the removal of this slowly varying altitude variation, to obtain a profile of surface elevation and ice morphology only. Different methods exist to perform altitude removal, and their application depends on the availability of additional, auxiliary data, for example, from differential GPS and inertial navigation systems. Standard high-pass filtering procedures are generally not adequate because there is some spectral overlap between ice and aircraft signals, and because the surface elevation is not normally distributed.

However, Hibler (1972) introduced a three-step filtering method to bypass this difficulty, which is followed by most studies in the absence of auxiliary data. First, a conventional high-pass filter is applied to identify minimum points along the high-pass-filtered time series, which represent locations with the lowest surface elevation along the profile, including open water. Then, a polygon connecting these low points in the original data set is constructed. The polygon is then low-pass filtered to represent the smoothly varying aircraft motion. Surface elevation results from subtraction of the measured distances from the reconstructed aircraft altitude (Figure 3.2.21).

It is important to note that due to the filtering process the obtained surface elevations do not represent the true surface elevations above the water level, but are relative to some datum, which typically follows the surface of the level ice. This implies that the obtained elevations are normally too inaccurate to calculate ice thickness from. However, surface roughness (i.e., the variability of the elevation profile) and in particular ridge distributions can be well determined. The latter can be identified from local maxima along the profile by some kind of Rayleigh criterion, which requires that the local elevation maxima are at least twice as high as the deepest points of the neighboring troughs (e.g., Hibler 1975). Ridges are only considered if their height exceeds a certain cut-off height of typically 0.8 m, for example, to avoid bias from smaller roughness features like snowdrifts or processing artifacts from floe edges.

From the height of the extracted ridges and their spacing, various statistical parameters can be derived, including mean ridge height and spacing, as well as ridging intensity, which is the ratio of mean height or squared mean height over mean spacing. From these, significant regional differences can be well determined (e.g., Dierking 1995; Granberg and Leppäranta 1999), which also provide important information for the validation of satellite data, particularly from synthetic aperture radar (SAR) (see also Chapter 3.15).

Most single-beam laser altimeters operate in the near infrared with a wavelength of 905 nm. Sampling frequencies range between 100 and 2,000 Hz, resulting in a spacing of 0.02 to 0.5 m between individual measurements, depending on flying speed. Distance can be measured with an accuracy of 0.01 to 0.05 m, and therefore even the small-scale roughness of the ice surface can be well resolved. Inaccuracies result mainly from pitch and roll of the aircraft, leading to slanted viewing angles, and from uncertainties in the aircraft altitude compensation. Laser altimeters are typically flown at altitudes of 30 to 300 m.

Improved Removal of Aircraft Altitude Variations

The problems due to aircraft motion are more severe for helicopters than for fixed-wing aircraft, which are much more stable in flight and whose altitude varies more slowly. However, altitude variations provide a serious problem for fixed-wing airplanes as well. Today, they can be measured independently with high precision using a combination of differential GPS and inertial navigation systems. These measure the position, altitude, and attitude of the aircraft (Hvidegaard and Forsberg 2002). Sea ice surface elevation Z_{se} is then obtained from $Z_{se} = h_{GPS} - h_{Laser} - N - \Delta h$ where h_{Laser} is the laser range, h_{GPS} the GPS-measured airplane height in a GPS reference system relative to an ellipsoid (e.g., WGS84), N is the geoid height, and Δh is a residual term describing the dynamic sea-surface topography due to tides, currents, and sea-level pressure variations (Figure 3.2.20). These terms are required because GPS heights are determined relative to a worldwide ellipsoid that does not represent the actual geoid at a given location. The geoid elevation N is obtained from a high-resolution geoid model, for example, from the Arctic Gravity Project (Forsberg and Skourup 2005).

The residual sea-surface topography term has magnitudes of less than 1 or 2 m and is of a long-wave nature (see also Figure 3.2.23). As the actual sea surface corresponds to the lowest points in the obtained surface elevation profiles, either from open water or newly frozen leads, similar filtering procedures as described above for stand-alone lasers can be used to remove the remaining bias. Local minima at leads or cracks can be identified as open-water tie points and can be connected to represent the actual sea level along the flight track (Hvidegaard and Forsberg 2002). This procedure also removes any residual bias due to possible laser offsets and misalignments, GPS errors, geoid errors, and the dynamic sea-surface topography. As all these residual biases vary only very slowly, surface

elevation can be obtained with an accuracy of between 0.05 and 0.13 m (Hvidegaard and Forsberg 2002; Forsberg and Skourup 2005). The uncertainty in derived ice thickness is approximately tenfold, and depends on assumptions about ice and snow density, and snow thickness (see Section 3.2.8.4). Accurate retrieval of ice thickness from measurements of surface elevations remains a major challenge (Hvidegaard et al. 2006).

As with multibeam, upward-looking sonar measurements (Section 3.2.8.1), two-dimensional information about the ice surface elevation can be obtained from airborne across-track laser scanning (Figure 3.2.22). Most laser scanners have across-track viewing angles of 45 degrees, resulting in a swath width approximately equal to the flying height. Measurements are performed at angular steps of, for example, 1.5 degrees, resulting in a spatial sampling rate of 1 m for a flying altitude of 300 m. The accuracy of individual measurements is comparable to those of single-beam lasers (i.e., ranges between 0.02 and 0.05 m). However, accurate correction of aircraft attitude variations by means of DGPS and inertial navigation system data is particularly important, as slight roll angles lead to lateral shifts of the laser swath and will result in wrong projections of each individual beam on a horizontal reference plane. Laser returns from open water are often spurious, depending on the wave-related roughness of the water surface and the amount of impurities in the water. However, with off-nadir beams this problem is even larger, as most energy is reflected away from the laser detector. This can be seen in Figure 3.2.22, where data gaps indicated by white filling exist in the regions of open water and thin, level new ice. Laser scanner data is particularly useful for the validation of lower-resolution airborne or satellite measurements which include information

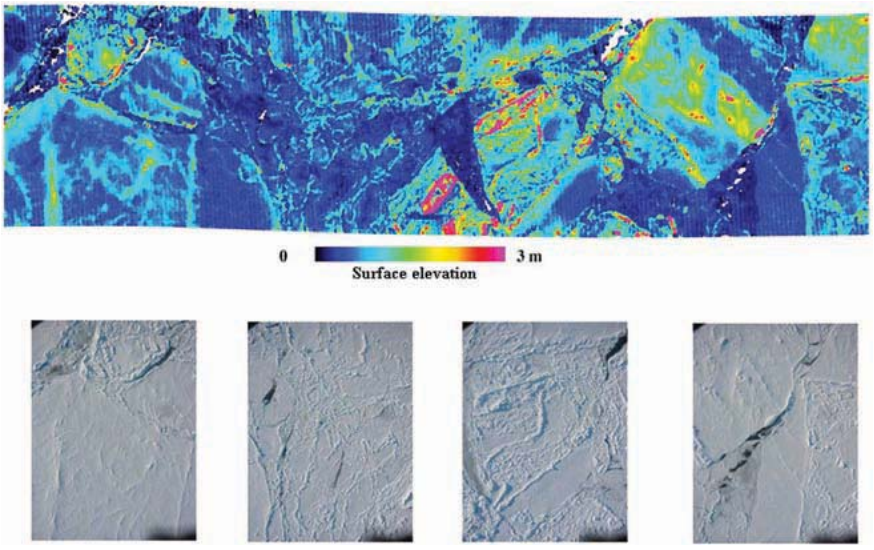

Figure 3.2.22. Typical laser scanner swath of the two-dimensional distribution of sea ice surface elevation, and comparison with aerial, nadir-looking photographs. The width of the swath is approximately 300 m (courtesy R. Forsberg).

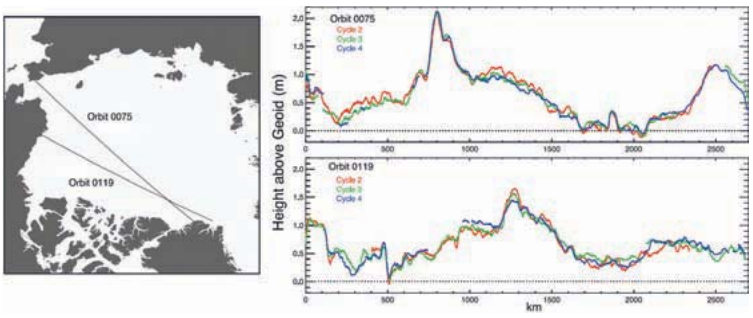

Figure 3.2.23. Sample elevation profiles across the Arctic Ocean from two exact repeat ground tracks of ICESat (see below), separated 8 days apart, and after removal of the best available Arctic geoid and tidal effects (Kwok et al. 2006). Large variations along orbits and between repeat-tracks can still be seen.

from the two-dimensional thickness distribution and roughness, as was shown with respect to airborne EM surveys (Hvidegaard et al. 2006) and ICESat surface elevation measurements (Skourup and Forsberg 2006).

To overcome some of the operational constraints, like limited operating time and range and high cost of manned aircraft, unmanned aerial vehicles (UAVs) have been used for airborne laser surveying as well, both with single-beam and scanning laser altimeters. Dedicated laser instruments are small enough to be carried by these vehicles, which generally have a limited payload. However, costs of these relatively new platforms are still very high, and it is not yet proven that their operational constraints are less than those of manned aircraft. There are also serious problems with air-worthiness and flying permissions.

3.2.8.4 Satellite Altimetry

Altimeters can also be operated from satellites to observe sea ice surface elevation or freeboard, which can be transformed into estimates of ice thickness. At first sight, satellite measurements seem to be superior over all other methods in their temporal and spatial coverage of the polar oceans. And this is certainly true if large-scale climate aspects of sea ice thickness are considered. However, for most other sea ice service applications, satellite altimetry is probably the least suitable method, due to constraints imposed by orbit geometry and survey repeat times. Altimetric measurements are essentially one-dimensional along the satellite track, and therefore there are large regions of the earth surface which are not covered by satellite altimeters at all. There are trade-offs between orbit inclination, repeat orbit intervals, and ground coverage. For example, higher across-track coverage can be achieved with longer repeat intervals, but then temporal changes cannot be so well resolved. A typical orbit repeat period is 30 days. More frequent measurements are

then only performed at cross-over locations of descending and ascending orbits. In addition, the uncertainty of individual point measurements can be large, and sufficient accuracy is only obtained with significant spatial and temporal averaging.

Satellite altimeters measure the distance between the satellite and the surface of the earth. Relative surface height differences between the ice and water are observed to estimate sea ice freeboard or surface elevation. In the absence of frequent open-water regions, the processing again has to rely on assumptions of linear changes of the local sea-surface topography between open-water tie points. Although orbit variations of satellites are much smaller and happen on longer spatial scales than altitude variations of airplanes, reconstruction of the local sea surface height as a datum for surface height measurements of the snow or ice surface is still a major challenge. Small-scale sea-surface height variations occur due to tides and currents, unknown geoid undulations, and temporal variations due to weather-related surface pressure changes (Figure 3.2.23). In addition, calculation of ice thickness from measurements of surface elevation or freeboard relies on several assumptions about snow thickness and density, as well as the densities of ice and snow.

Two different kinds of instruments exist: radar and laser altimeters. These are generally different in their penetration characteristics for snow and sea ice, and in their spatial resolution. Their different penetration characteristics are particularly important for sea ice measurements. While the near-infrared wavelengths of lasers do not penetrate into snow and ice and are scattered at the upper surface, radar altimeter wavelengths, typically at Ku-band (e.g., 13.8 GHz or 2.2 cm), penetrate the snow to some degree, and the reflections are generally believed to originate from the snow-ice interface (Laxon et al. 2003). Therefore, with laser altimeters the elevation of the snow surface Z_{se} is obtained, while with radar altimeters the freeboard Z_{fb} of the ice is retrieved (cf. Figure 3.2.4). Accordingly, different equations for the calculation of ice thickness z_i result from Archimedes' law and the general isostasy,

$$z_i = \left(\frac{\rho_w}{\rho_w - \rho_i}\right) z_{se} - \left(\frac{\rho_w - \rho_s}{\rho_w - \rho_i}\right) z_s$$

$$\text{For laser altimetry:} \quad z_i = \left(\frac{\rho_w}{\rho_w - \rho_i}\right) z_{fb} - \left(\frac{\rho_s}{\rho_w - \rho_i}\right) z_s \quad \text{(Equation 3.2.6a)},$$

$$\text{For radar altimetry:} \quad z_i = \left(\frac{\rho_w}{\rho_w - \rho_i}\right) z_{fb} - \left(\frac{\rho_s}{\rho_w - \rho_i}\right) z_s \quad \text{(Equation 3.2.6b)},$$

with the densities ρ_w, ρ_i, and ρ_s of water, ice, and snow, respectively, and snow thickness Z_s.

With typical densities of ρ_w = 1,024 kg/m^3, ρ_i = 925 kg/m^3, and ρ_s = 300 kg/m^3, the first term in these equations implies an approximately tenfold amplification of freeboard uncertainties for the calculation of ice thickness for both methods. However, it is also important to note that the second terms are different, resulting in a stark difference in the sensitivity of thickness retrievals to uncertainties in snow thickness. The term is approximately 7 for laser altimetry and approximately 3 for

radar altimetry. Therefore, snow thickness uncertainties in laser altimeter data contribute to more than twice as large uncertainties in retrieved ice thicknesses than in radar altimeter data.

A comprehensive analysis of the sensitivity of ice thickness calculations according to Equations 3.2.6a,b to uncertainties in snow and ice properties has been performed by Kwok and Cunningham (2008). While snow thickness on arctic sea ice is generally derived from a climatology compiled by Warren et al. (1999), Kwok and Cunningham (2008) show that improved estimates of snow thickness can be obtained from reanalysis models from the European Center for Medium Range Weather Forecast (ECMWF). In addition, the authors show improved analyses of seasonal changes of snow density. With these, the overall uncertainty of thickness retrievals from altimetry can be reduced to less than 0.7 to 0.5 m. More discussions of the comparison of surface elevation and ice draft can also be found with Wadhams et al. (1992), who compared draft and surface elevation data obtained along coincident tracks of a submarine and an airplane.

Radar Altimetry

Radar altimeter observations of sea ice were first performed with Seasat in 1978, and more routine observations are available from ERS-1 and ERS-2 since 1991. Since 2002, radar altimetric measurements over sea ice are obtained by Envisat. These measurements are generally limited to sea ice regions south of 81.5° N and north of 81.5° S due to the inclination of the satellite orbits of 98.5° at best. In late 2009, the European Space Agency will launch CryoSat, a dedicated ice radar altimetry mission, which will obtain measurements up to 88° N and S. The ERS altimeter had a pulse repetition frequency of 1,020 Hz. Fifty pulses were averaged into one waveform (see below) to yield an effective sampling interval of 0.49 s, corresponding to a point spacing of approximately 330 m on the ground. Note that the point spacing is much smaller than the footprint (see below).

General aspects and details of radar altimetry and sea ice measurements are described by Fetterer et al. (1992). Satellite radar altimetry is routinely employed to measure sea surface heights and wave heights over open oceans. Satellite altimeters use pulse-width-limited geometry, where a pulse of microsecond-scale length is emitted within a < 1-degree-wide beam. The pulse echo returned from the surface of the earth is received with temporal resolution of the energy arriving back at the satellite. The area on the surface illuminated by the pulse grows with time, until the trailing edge of the pulse leaves the lowest reflecting points at nadir. The maximum area simultaneously illuminated is usually referred to as pulse-limited footprint, and depends on the roughness of the surface. It can vary between one and several kilometers in diameter. Returns received at later times represent energy scattered back from off-nadir locations. The data set of received energy versus time is generally referred to as waveform, and its shape and instance are used to assess the distance to and characteristics of the earth surface.

Over sea ice regions, most waveforms are very narrow with high power. This is a result of specular reflection from small fractions of smooth open water or nilas in cracks or leads with high backscatter within the large footprint (Peacock and Laxon 2004), which reflect rather than scatter the radar energy back to the satellite. The resulting "peakiness" of waveforms can be quantified and is a powerful separator between ice-covered and open ocean (Fetterer et al. 1992). However, when the footprint is entirely covered by ice, diffuse waveforms occur within the sea ice zone as well (Laxon et al. 2003; Peacock and Laxon 2004). This is usually observed in less than 5 to 10 percent of all measurements, depending on season and ice conditions. The different height retrievals from specular and diffuse waveforms within the sea ice zone can then be used to determine the surface heights of the water and ice surfaces, whose difference is freeboard.

The construction of the sea surface from specular waveforms is not straightforward, as it is generally unclear which time instance of the waveform represents the distance to the pulse-limited footprint region at nadir. This instance is normally determined by the satellite electronics based on diffuse waveforms and the time history of previous waveforms, and can vary on short and longer time scales along the orbit (Peacock and Laxon 2004). Therefore, extensive, sea ice–specific reprocessing ("retracking") of waveforms is required to reduce the noise. Additional low-pass filtering is applied, and then the resulting profiles of sea-surface height have noise levels of less than 0.25 m (Peacock and Laxon 2004). Diffuse waveforms are treated similarly, and freeboard is obtained from the height differences obtained from specular and diffuse waveforms (Laxon et al. 2003). Ice thicknesses of less than 1 m are normally excluded from the analysis as their freeboard is too small to be discerned with high confidence. The details of the processing vary with sensor characteristics and ice conditions, and also have to include corrections for radial orbit errors and tropospheric and ionospheric effects. They generally require some fine-tuning. For example, in the Arctic freeboard can often only be retrieved between October and March, as broken-up ice fields and a wet, melt pond–covered ice surface significantly reduce the number of diffuse reflections and radar backscatter. Statistical accuracies are further improved by spatial and temporal averaging, e.g., over 0.25 × 0.25 degree grid areas and monthly fields. With this, Laxon et al. (2003) estimate their ice thickness accuracy to be within 0.11 m to 0.2 m, which implies an accuracy of their freeboard retrieval of 0.01 to 0.02 m, according to Equation 3.2.6b.

A thorough validation of satellite radar altimetry thickness retrievals is pending. However, Figure 3.2.24 shows a comparison of radar-altimeter-derived thicknesses with results from ULS profiling. Large uncertainties are visible both with individual radar altimeter and ULS data points, pointing to scale-related problems due to the differing footprints of radar altimeter and ULS measurements. On a large-scale, long-term average, however, radar altimeter retrievals of ice thickness seem to have a high accuracy. This is also indicated by the linear least-square fit in Figure 3.2.24, which yields a slope of 0.98 and intercept of 0.12 m (Laxon et al. 2003).

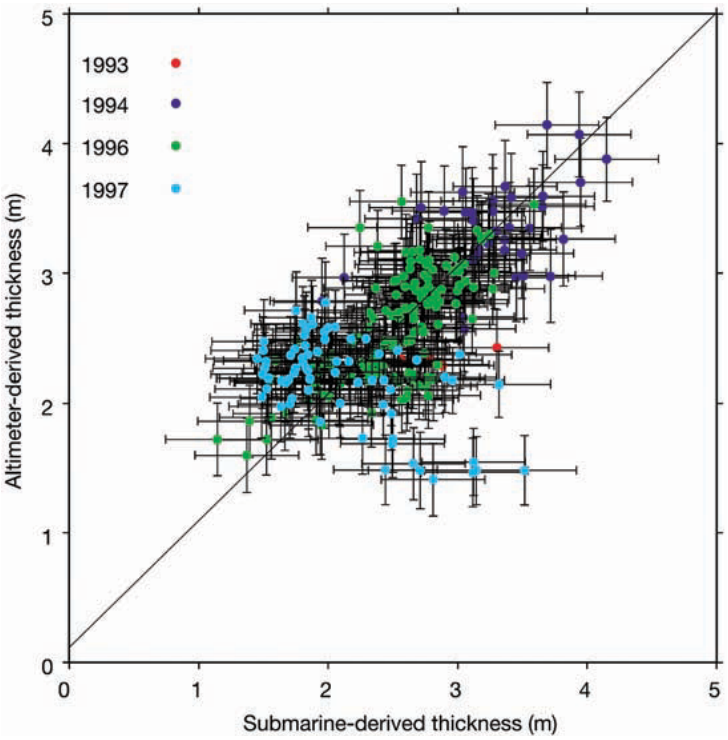

Figure 3.2.24. Comparison between satellite altimeter and submarine ULS-derived ice thickness in the Beaufort Sea (Laxon et al. 2003). Submarine thicknesses are shown for 50-km profile segments gathered during four missions. Altimeter thickness estimates were generated from observations within 15 days and 100 km of the submarine tracks. Submarine thicknesses exclude ice thinner than 0.5 m and open water, because (owing to difficulties in discriminating thin ice from open water) progressively less altimeter data can be retrieved once thickness falls below 1 m. Error bars show uncertainties in altimeter thickness due to measurement errors and snow depth variability and an error in submarine thickness of 0.4 m. Diagonal line shows result of a least-squares fit (see text).

Laser Altimetry

A satellite laser altimeter has so far only been launched once, and is still operating (as of April 2009) onboard the ICESat satellite launched in 2003. Its Geoscience Laser Altimeter System (GLAS) operates with a laser wavelength of 1,064 nm to profile the Earth's surface (Zwally et al. 2002). With a beam width of approximately 110 mrad and a pulse rate of 40 Hz, it obtains a measurement approximately every 170 m with a footprint diameter of 70 m. The orbit inclination is 94 degree, allowing surveys up to 86° N and S. Due to the narrowness of the beam, accurate attitude determination is very critical, in addition to the general necessity of precise orbit determinations. Unfortunately, there were technical problems with the

laser systems of ICESat, which have limited its operation to February-to-April and October-to-November seasons; however, this is still sufficient for the observation of seasonal ice thickness variations.

As with radar altimeters, not only the travel time of the emitted laser pulse between satellite and the earth surface is recorded, but also its time-dependent return at the laser receiver. The resulting waveforms are analyzed for width and amplitude, allowing conclusions on surface roughness and reflectivity (Zwally et al. 2002). The wider the received waveform, the rougher the surface.

The ability to determine surface reflectivity can be ideally used to delineate regions of snow-covered ice and new ice or open water, as they are characterized by high and low albedos, respectively, even in the 1,064 wavelength range (Figure 3.2.25). Therefore, open water can be detected from regions of low reflectivity, and can be used as tie points for the reconstruction of sea level (Kwok et al. 2006). Figure 3.2.25 shows that low reflectivity of a newly opened lead coincides with a region of the lowest surface elevation as expected. The figure also shows that there are additional regions of thinner ice identified by their low surface elevation, which do not have lower reflectivities. These represent younger ice, which is already snow covered to some extent. The figure illustrates that these low-level locations could be mistakenly identified as open water or new ice if no other,

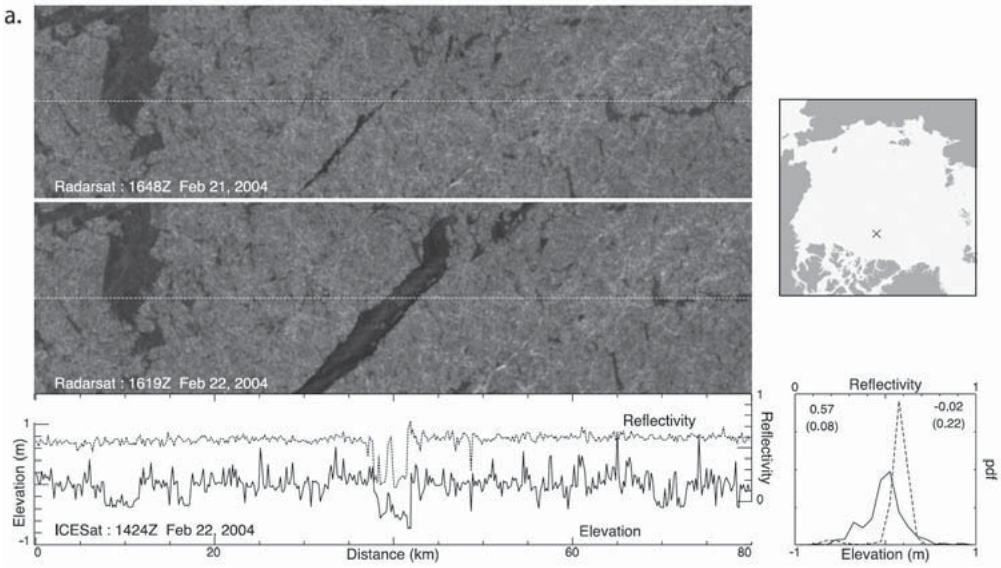

Figure 3.2.25. Example of 80 km long ICESat profile from the Arctic Ocean (cross on map) and comparison with near-coincident Radarsat SAR images (from Kwok et al. 2006). The SAR images were obtained one day apart, and show the opening of a new lead in the center of the image, visible by its low backscatter (dark color). The ICESat track is shown as white dashed line. The overflight took place only two hours before the acquisition of the lower image. Lower panel shows the elevation (solid, centered around mean) and reflectivity profiles (dashed). The bottom right panel shows the distributions of elevation and reflectivity, and their mean and standard deviations (numbers).

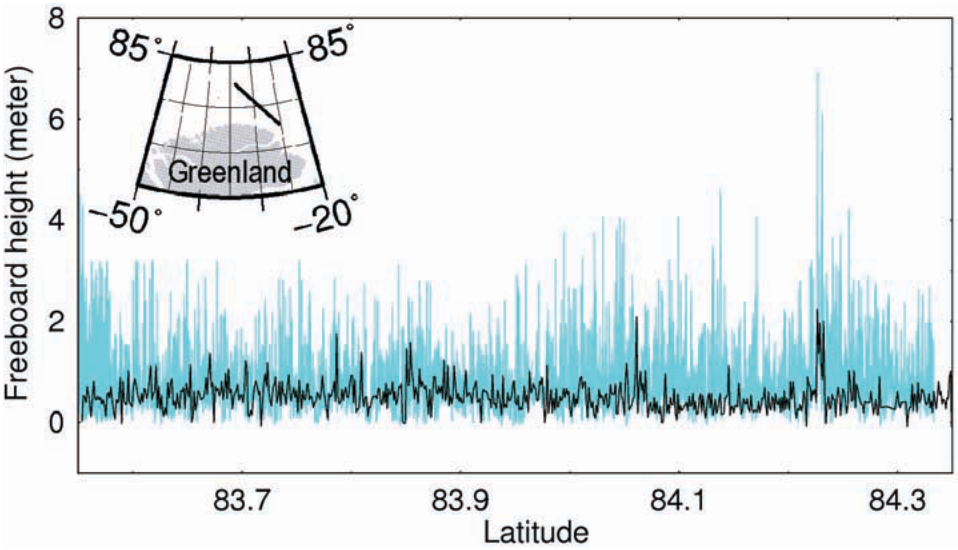

Figure 3.2.26. Comparison of freeboard heights from airborne (blue) and satellite (ICESat; black) laser altimetry. The inset map shows the track location north of Greenland (from Forsberg and Skourup 2005).

even lower locations would be observed. Only with proper reflectivity information can open-water locations be clearly identified. Experience shows that usually there is some occurrence of open water along profiles of 25 km length, which is normally taken as the minimum distance over which at least one tie point should be observed (Hvidegaard and Forsberg 2002; Forsberg and Skourup 2005; Kwok et al. 2007).

Overall, Kwok et al. (2007) estimate that the uncertainty of ICESat freeboard retrievals along 25 km segments is better than 0.07 m on average. Again, validation of these results is difficult due to the spatial and temporal scales and the different footprints. Figure 3.2.26 shows two 80 km long, coincident ICESat and aircraft laser profiles (Forsberg and Skourup 2005). Sea level has been derived from an along-track lowest-level filtering scheme with a resolution of ~15 km, neglecting reflectivity information in the ICESat data. Both profiles are in good qualitative agreement. However, the height of lowest levels differs by ~25 cm. This difference is due to the large footprint of ICESat of 70 m, which prevents the detection of narrow leads or cracks. Similarly, individual pressure ridges cannot be profiled, as they are averaged over the footprint area.

Figure 3.2.27 shows another example for the validation of ICESat thickness retrievals (Kwok and Cunningham 2008). ICESat freeboard has been retrieved with more sophisticated methods than for the example in Figure 3.2.26, using SAR images and reflectivity information for the determination of open-water tie points (see above). Ice draft has been calculated with the best available estimates for snow thickness and snow and ice density (Kwok and Cunningham 2008). Results are

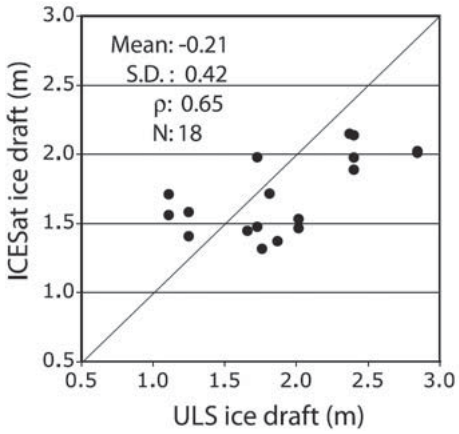

Figure 3.2.27. Comparison of mean ICESat and ULS draft retrievals for overlapping and coincident, 25 km long profiles (Kwok and Cunningham 2008).

compared with moored ULS measurements, which have been temporally averaged to be comparable with 25 km long ICESat profiles. Taken together, the overall difference between ICESat and ULS draft estimates is –0.21±0.42 m, with a correlation of 0.65 between the two ice draft populations (Figure 3.2.27).

With both satellite radar and laser measurements, the question remains to be answered whether the surface elevation retrievals represent mean ice thickness, modal ice thickness, or some other measure of the thickness and morphology of the ice. As the modal ice thickness represents the thickness class with the largest areal coverage (Section 3.2.1), it would be plausible that the instance of maximum energy return at the satellite receiver agrees with the two-way travel time to the level ice surface. In contrast, ridges contribute to the roughness of the ice surface, and their high elevations should lead to earlier arrivals and higher energy of the leading edge of the received waveforms.

3.2.9 ICE THICKNESS MEASUREMENTS FOR VARIOUS SEA ICE SERVICES

3.2.9.1 Ice Thickness Measurements for the Detection of Climate Variations

Sea ice is a regulator of the global climate, and its thickness is an indicator for the state of the climate in the polar regions and its variability. Ice thickness measurements have to be performed in a systematic manner and over long times to detect climate changes, given the large seasonal and interannual variability of sea ice and the redistribution of thick and thin ice to different regions. There are many examples of observations of ice thickness changes on various scales, ranging from long-term point measurements on fast ice using drill holes, to long time series of moored ULS measurements and submarine ULS profiles. The arguably most spectacular changes have been reported from a comparison of U.S. submarine cruises performed in the period 1958–1976 with data from the 1990s (Rothrock et al. 1999) (Figure 3.2.28). Overall, ice thickness has decreased by 1.8 m between periods—a

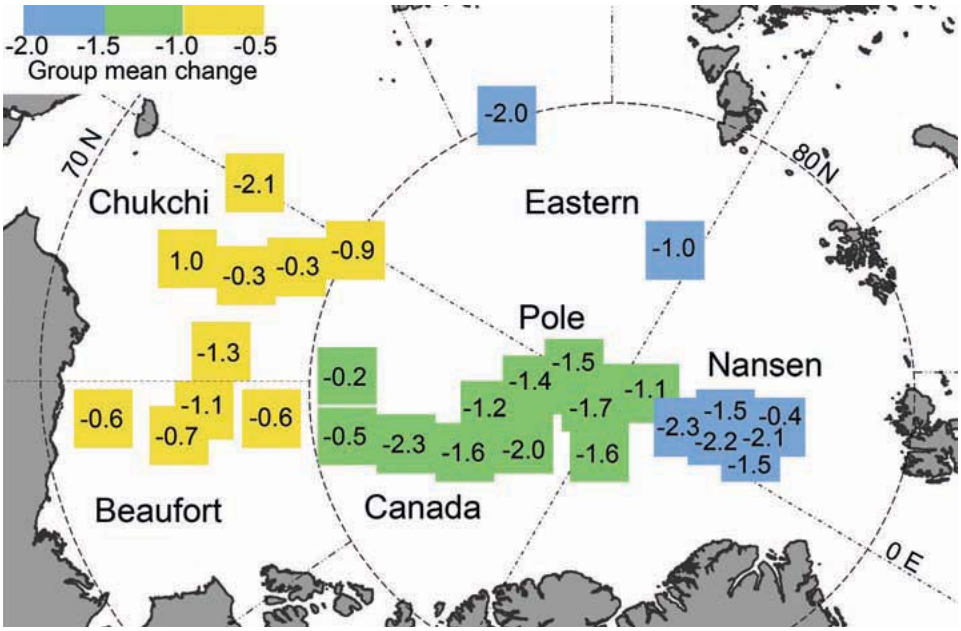

Figure 3.2.28. Changes in mean ice draft between the periods 1958-1976 and 1993-1997 (Rothrock et al. 1999). Boxes show regions of 150 km width, over which overlapping data between both periods have been compared.

thinning of 42 percent from a mean of 3.1 m. Apart from the average decrease, all regions with overlapping data showed thinning, which was strongest in the eastern Arctic and least in the Beaufort Sea (Figure 3.2.28). However, model studies showed later that the interpretation of the changes is difficult because data were obtained only sporadically within the compared periods, and because only the central region of the Arctic Ocean over which data were declassified could be analyzed. This did not allow the detection of redistribution of thick ice within the whole Arctic, and particularly towards the coasts of Greenland and Canada.

Another example of observations of most recent, climate-related thickness changes in the region of the North Pole is given in Figure 3.2.29 (Haas et al. 2008a). Data was obtained by means of ground-based and helicopter-borne EM sounding, using an icebreaker as a moving base to provide a large, regional observational range. Results show another rapid reduction of modal and mean thicknesses of 53 and 44 percent between 2001 and 2007, respectively. Again, data have only been obtained in six summers over a 17-year period, because icebreakers are not regularly available for this kind of research. Therefore, the interannual variability cannot be derived from the measurements to better confine the trend. Also, data from April 2007 had to be seasonally adjusted for comparison with the summer measurements in order to account for seasonal changes due to ablation during the melting season. However, with additional data now available from buoys, satellites, and meteorological reanalyses, the causes of the thinning can be much better identified. Figure

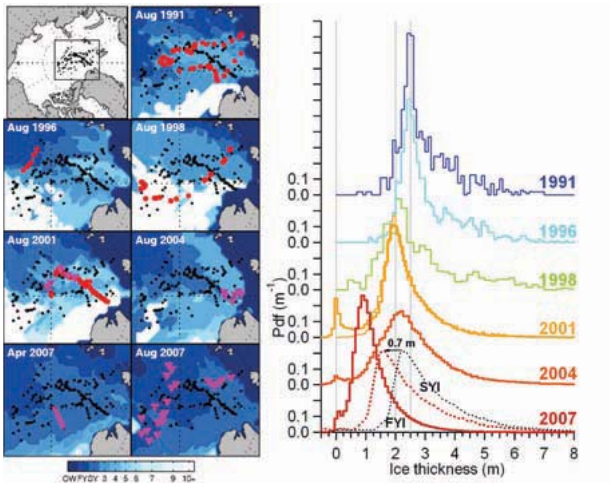

Figure 3.2.29. Late summer ice age (left) and thickness (right) change in the region of the North Pole between 1991 and 2007 (Haas et al. 2008a). Thicknesses were obtained by means of ground-based (thin lines, red circles) and HEM sounding (thick lines, magenta triangles). The second-year ice (SYI) distribution obtained in April 2007 was seasonally adjusted by 0.7 m to represent summer conditions (Haas et al. 2008a).

3.2.29 shows that the observed thinning is accompanied by a reduction of the age of multiyear ice, and even by a replacement by first-year ice in the study region. Presentation of thickness distributions like in Figure 3.2.29 and analyses of decreasing modal thicknesses also allow for conclusions that much of the observed thinning is due to changes in thermodynamic boundary conditions. However, these observations alone do not allow us to judge whether the thinning is due to changes in atmospheric or oceanic boundary conditions, or both. Nor can conclusions be drawn on the importance of reduced winter growth or summer ablation for the observed thinning. Ideally, these measurements should be accompanied by observations from ice mass balance buoys (Section 3.2.6), or they should be performed at least twice a year, at the end of the freezing season (April/May) and ablation season (September).

3.2.9.2 Thickness Measurements in Support of On-Ice Travel, Subsistence, Ice-Runway Preparation, and Biological-Physical Process Studies

Travelers on sea ice, whether they be local hunters on foot or snowmachine, engineers designing ice roads, or scientists conducting field campaigns, are often very concerned with both ice thickness and roughness. Ice thickness is directly related to ice's load-bearing capacity and integrity; ice thickness and surface roughness determine whether ice is stably grounded in shallow waters; and surface roughness has clear implications for trafficability—the ability of a given traveler to traverse the ice cover. Although sea ice users may have differing understandings of how ice properties relate to these on-ice travel and operational concerns, general relationships do exist and can often be informed by the measurement techniques discussed in this chapter.

When determining whether or not ice of a given thickness will support an activity on the ice, one must consider a number of variables. Given the viscoelastic response of ice to an applied load, both the weight of the load and the rate of

loading are important. Also when transporting a heavy load across level ice, one must consider how speed relates to wave dynamic responses in the water beneath the ice that may contribute to failure. The load-bearing capacity of ice depends on ice type (first year or multiyear), temperature, salinity, porosity, stress history, and cracks and nonhomogeneities (Potter and Walden 1981). These variables also have implications for how a given piece of ice will withstand longitudinal pressures imparted by adjacent ice. While knowledge and formulas used to evaluate strength and load-bearing capacities vary in sophistication and are typically derived empirically, ice thickness is perhaps the most important variable and also the easiest and most straightforward to measure.

Grounded sea ice ridges, which may be thought of as roughness on the scale of 10^0 to 10^1 m, play a fundamental role in whether or not landfast sea ice may be considered stable from an ice user's perspective. Of importance to travelers on ice are break-out events in which large sections of ice are destabilized and detach from the coast or from other remaining sections of landfast ice. For example, throughout history and continuing into the present day, such events have presented a significant threat to hunters traveling on sea ice in the coastal regions of the Arctic (George et al. 2004). Grounded ridges may be either formed in place through deformation or may be advected in from elsewhere and deposited. Assessing the stability of landfast sea ice is very complex as it is influenced by a range of interacting variables—sea-level fluctuations, water temperature, currents, winds, ice morphology, salinity, pack ice interaction, and "weak spots" or cracks within the ice. In general, the presence of grounded ridges within the landfast ice cover, most of which is typically floating, contributes to its ability to resist destabilizing forces. However, in some cases, the keels of weakly grounded ridges may in fact contribute more to a potentially destabilizing drag by the current than to serving as anchoring points (Mahoney et al. 2007).

Roughness on scales ranging from 10^{-2} to 10^1 m typically has implications for trafficability. During the construction of groomed sea ice roads or airstrips, the ice surface is leveled, often with a bulldozer, and then flooded to create a smooth path. Here, concerns may exist on the centimeter scale as even small cracks and inhomogeneities may negatively impact traffic or the integrity of the surface. Those traversing an unaltered ice cover are impacted by features ranging from light rubble (dimensions < 1 m), which presents obstacles as well as promotes snowdrifts capable of concealing cracks, to ridges of sail heights from one to tens of meters (Barker et al. 2006). Industrial operations on offshore structures in arctic landfast ice are interested in how roughness and rubble conditions relate to the efficiency of emergency evacuation plans where people leaving the primary structure must traverse a range of conditions to reach on-ice evacuation shelters (Barker et al. 2006), or to escape to otherwise safe conditions.

As discussed in Section 3.2.8 satellite data has clear limitations for obtaining ice thickness information. However, when using a satellite image of an area where

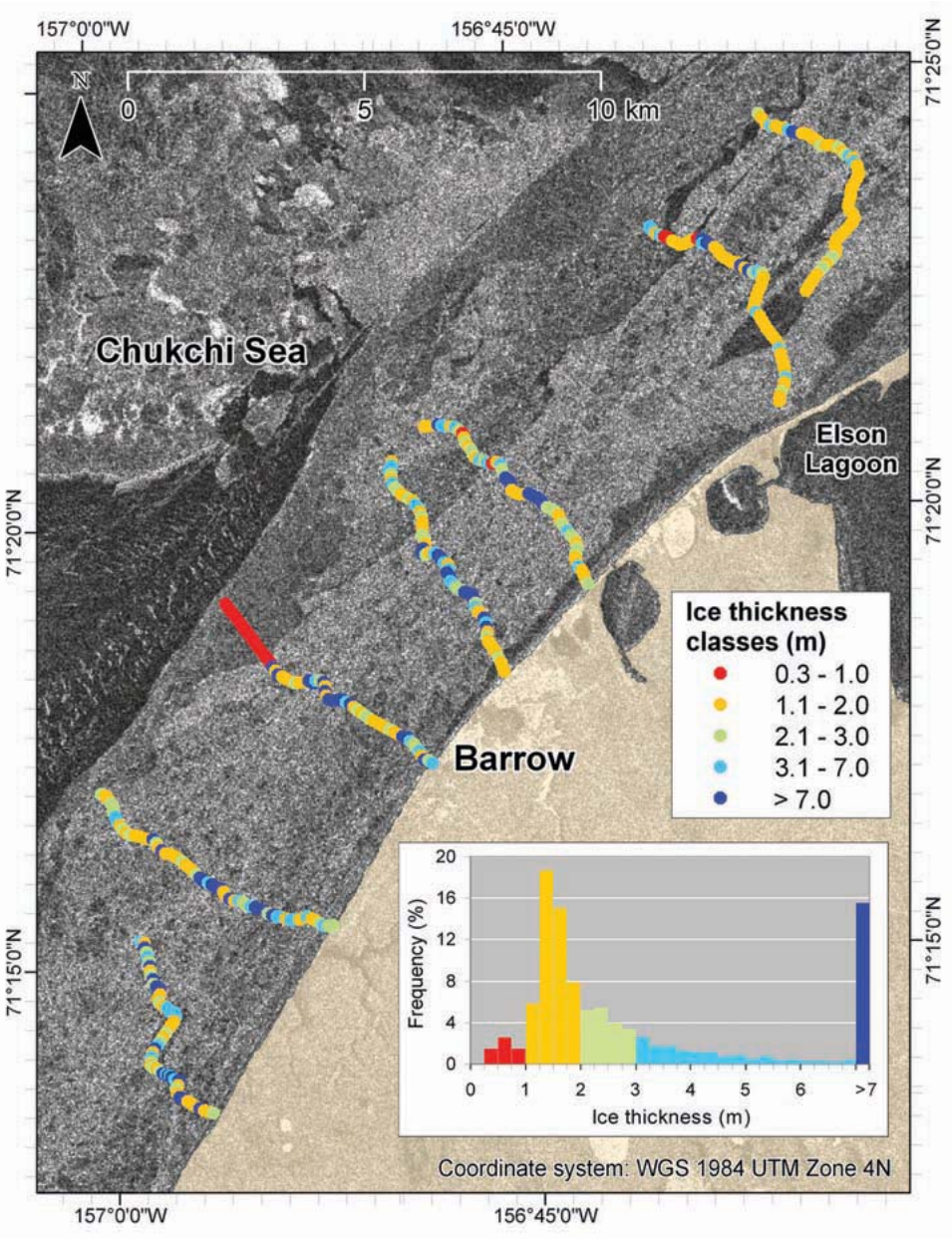

Figure 3.2.30. EM-derived ice thickness measurements along trails constructed by Iñupiat whale hunters on the landfast ice off Barrow, Alaska in spring 2008. Trails originate near land and traverse a range of ice types before terminating at the lead edge where hunting camps are established. (The background of this map is an ERS-2 SAR satellite image from 22 March 2008. The semi-transparent yellow overlay represents land.)

extensive ice thickness measurements have been made using other methods, one can extrapolate thickness information from one area to another based on the information in the satellite image. Figure 3.2.30 presents a spatial plot of EM-derived ice thickness measurements along trails constructed on the landfast ice off Barrow,

Alaska, in spring 2008 during the bowhead whale hunt by Iñupiat whalers. These measurements were made by hauling an EM device, similar to that shown in Figure 3.2.13, on a small sled along the trails. The thickness data presented here shows the thickness distribution of the sampled ice, but also lends insight into how to interpret the SAR satellite image that the data overlies. In general, smooth and relatively thin ice is represented by areas of low radar backscatter (darker areas), such as the region overlaid by measurements of ice thickness less than 1 m (indicated by red dots) in the center left side of the figure. The thicker, rough and highly deformed ice is represented by the areas of higher backscatter (brighter areas). A stretch of thick ice (indicated by the light and dark blue dots), which is largely composed of ridges thicker than 7 m, parallels the coast and intersects the five southernmost trails. Satellite information coupled with thickness data along trails may inform decisions regarding the trafficability of the ice in areas where trails do not exist. For example, thinner ice of low backscatter may provide for efficient and nonobstructed timely travel as opposed to areas of higher backscatter.

Figure 3.2.31 shows a similar example of an EM profile obtained by hauling an EM instrument with a skidoo between individual observational sites on an ice floe, overlaid on an aerial photograph (Haas et al. 2008c). The thickness measurements were used to delineate individual regions of the ice floe with the same properties

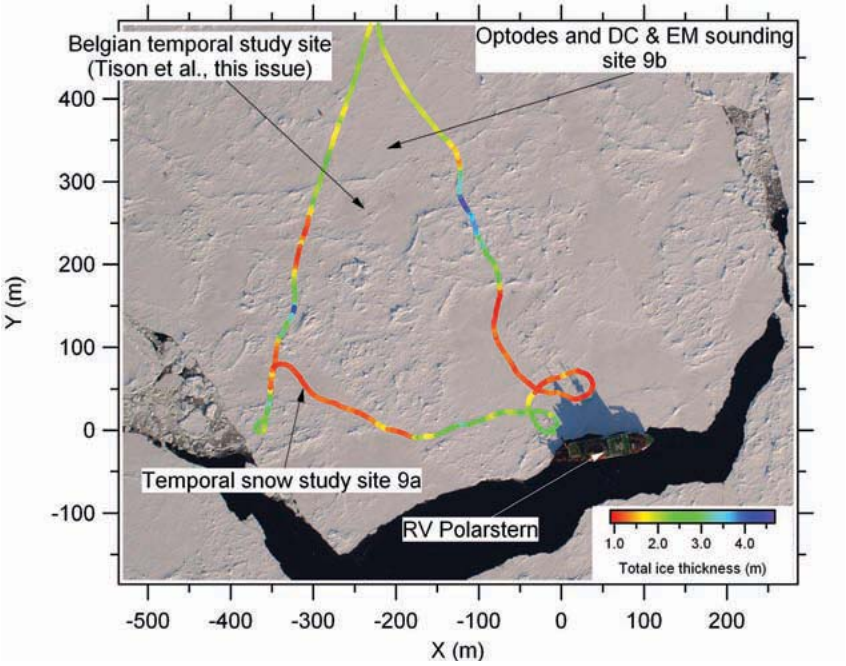

Figure 3.2.31. Nadir-looking aerial photograph of an ice floe in the Weddell Sea (Haas et al. 2008c; see also Chapter 3.17). Color-coded line shows ice thickness profile along a skidoo track connecting various sampling sites. Note composition of ice floe of thick rough SYI floe fragments and grayish, smooth thin FYI in between.

and developmental history, to support the interpretation of ice cores and other samples taken at the various sites for biological and glaciological studies (see also Chapter 3.17). Repeat surveys were also performed over a period of five weeks to study temporal changes due to progressing melt. The figure shows the presence of three ice types: smooth, thin first-year ice with total thicknesses of 1.0 to 1.2 m; medium smooth, thick first-year ice with total thicknesses around 2.0 m; and deformed second-year ice thicker than 2.5 m.

Obviously, these measurements are also efficient for pre-site surveys of ice floes for any kind of activity. They have been used to find thin ice regions for the deployment of buoys or divers, or for biological under-ice studies, where large holes have to be drilled into the ice, and where finding the thinnest ice causing the least trouble for producing those holes is of utmost interest. On the contrary, continuous EM surveys can be used to quickly and accurately profile regions of anticipated ice runways for aircraft operations, for which a homogeneous, thick enough ice cover has to be confirmed.

3.2.9.3 Ice Thickness Measurements in Support of Ship Performance Studies

In the design of icebreakers and definition of shipping regulations, knowledge of the performance of ships in ice is a prime requirement. Mostly, icebreakers are evaluated and classified according to the speed they can maintain in level ice of a certain thickness. Full-scale tests are performed in fast ice zones, where ice thickness is relatively uniform and determined by a few drill-hole measurements. However, the results of those tests can be misleading when transferred to real sea ice conditions, which may include a mixture of ice floes of different sizes and age, and pressure ridges. With the same ice thickness, ship performance in a neutral or divergent ice field can be much better than in a convergent ice field under pressure. The ship performance trials of the U.S. Coast Guard Cutter *Healy* in April and May 2000 in individual ice floes in Davis Strait and Baffin Bay were probably among the most comprehensive trials ever held and integrated a number of the methods presented above to measure ice thickness and roughness. These included the rotating laser level, mechanical ice drilling, ground-based EM surveys, hot-water drilling, and snow depth surveys as well as over-the-side video to document ice thickness (Sodhi et al. 2001). However, on scales of an ice field, ice thickness measurements by traditional means are very challenging, as it is difficult to traverse on foot or by skidoo across a mixture of ice floes, brash ice, and open water leads.

Therefore, ice thickness measurements have been performed by means of shipborne EM sounding in front of icebreakers sailing through ice (e.g., Haas 1998). As with helicopter-borne EM thickness sounding, the EM instrument has been accompanied by a laser altimeter to measure its elevation above the ice surface. Note that for relatively small distances of 4 to 8 m above the ice, sonic range finders can also be used. Here, a Geonics EM31 (Section 3.2.3) has been used, and both

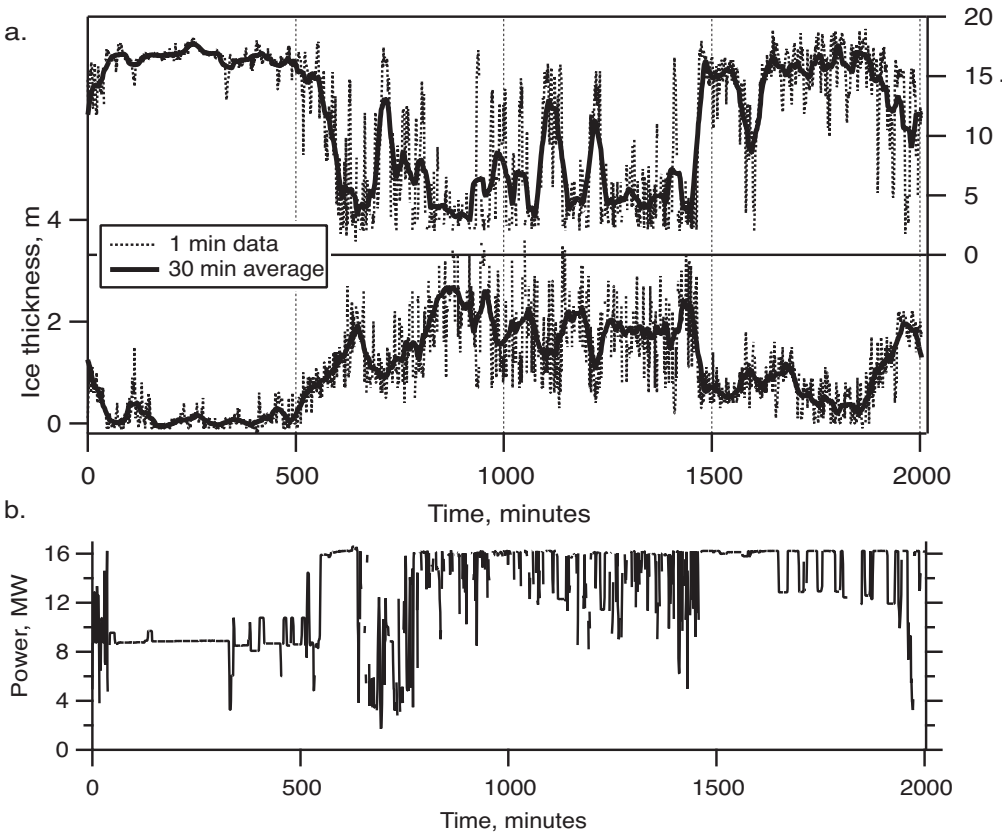

Figure 3.2.32. Ice thickness, ships speed (a) and delivered power (b) along a 33 hours long profile in the Kara Sea (Haas et al., 1999). Shown are 1-minute data as well as 30-minute running averages.

instruments were suspended from the ship's bow crane at an elevation of 4 m above the ice surface. Figure 3.2.32 compares ice thicknesses thus derived over a 33-hour period with ship's speed and delivered power (Haas et al. 1999). The data was obtained during the Arctic Demonstration and Exploratory Voyage (ARCDEV) of the Russian icebreaker *Kapitan Dranitsyn* in April 1998 in the first-year ice region of the Kara Sea. The icebreaker had accompanied an ice-capable oil tanker to load crude oil at a port on the Yamal Peninsula, and to deliver it to the European market. It can be seen that the ship speed decreased drastically as the ship entered more severe ice conditions, and was very low for the thickest ice. The relationship is visible in more detail in Figure 3.2.33, showing scatter plots of velocity and thickness for 1- and 30-minute averaging intervals. The correlation between the data is good ($r = 0.81$ and $r = 0.92$, respectively). However, the scatter for 1-minute data is very large. Note that with a speed of 10 knots, 1 minute of data corresponds to a profile length of approximately 300 m (i.e., two to three times the ship length). This scatter is significantly reduced for 30-minute averaging intervals.

There are various reasons for the strong scatter. Even despite the footprint of the EM method, the across-track ice area contributing to the measured ice thickness

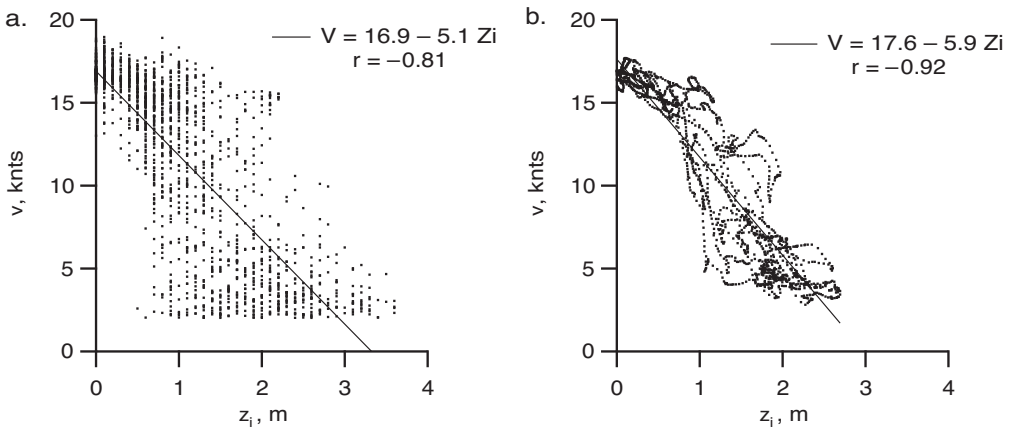

Figure 3.2.33. Mean speed V versus mean ice thickness Zi from Figure 3.2.32 for 1-minute intervals (a) and 30-minute running averages (b) Haas et al. 1999). The lines show a linear regression, and the resulting equations are given as well as the correlation coefficient r.

(~12 m) was less than the width of the ship (~25 m). In addition ice conditions in front of the ship were extremely variable, and the momentum of the ship made it less sensitive to small-scale variations. However, over longer periods, these variations contribute to a more uniform relationship.

Apart from evaluating the performance and design of an icebreaker based on the results shown in Figure 3.2.33, the relationship can also be used for the development of ship performance models to predict navigation times and speeds under certain ice conditions.

Thickness and properties of the snow can also be determining factors for the performance of ships. Sometimes, one-third of the snow thickness is added as effective, snow-related ice thickness to the true ice thickness. Obviously, snow thicknesses cannot be obtained from the EM measurements, and have to be observed independently.

3.2.9.4 Ice Thickness Sounding in Support of Ice Load Measurements

Like icebreakers (Section 3.2.9.3), any offshore structure located in drifting pack ice is subject to variable ice forces and needs to be designed to withstand them. Ice forces on structures are determined by the width of the structure, by the properties and speed of the ice, and by ice thickness. Within the European Union projects Low-Level Ice Forces (LOLEIF) and Structures in Ice (STRICE), attempts were made to relate ice forces to environmental conditions including ice thickness. Therefore, a lighthouse in the drift ice zone of the northern Baltic Sea was equipped with load panels at water level, a ULS, and an EM system (Figure 3.2.34) (Haas and Jochmann 2003). The ULS was located at a depth of 6 m below the water level, and was repeatedly damaged by ridge keel scouring. The EM system comprised an

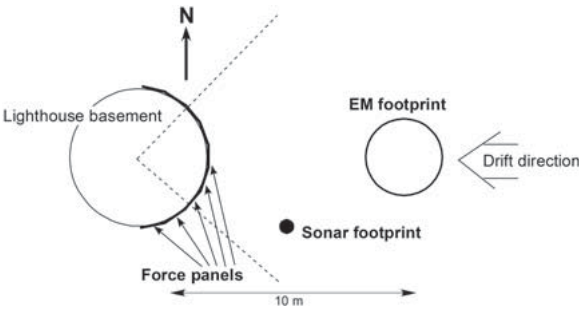

Figure 3.2.34. Sketch of an instrument setup to measure ice forces and their relation to ice thickness, showing the cross section of a lighthouse equipped with force panels as well as the locations of EM and ULS thickness measurements (Haas and Jochmann 2003).

EM31 conductivity meter (Section 3.2.3) and a sonic range finder. It was suspended 2 m above the ice by a scaffolding boom. Unfortunately, it was located some 5 m farther away from the lighthouse than the ULS. All data were recorded in real time and were visible on the lighthouse as the ice was passing by, shaking the lighthouse heavily as the ice crushed.

Figure 3.2.35 shows a time series of ice forces and associated ULS and EM ice thicknesses for a typical drift and deformation event. The forces show typical events of low-frequency, long-lasting static loads, with superimposed, up to five times stronger spontaneous loads due to crushing and/or bucking and bending failure. There is strong correlation between static ice forces and thickness in the example. However, peak forces due to crushing and bending failure blur a clear relationship, and can be very high in level ice and even higher than in ridges, as for example, around 07:00 h in the example. Figure 3.2.35 indicates that these peak forces resulted from virtually level zones of about twice the level ice thickness, which have been formed by rafting of the original ice cover and have not developed keels of very thick ice.

The measurement configuration also provided the unique opportunity to compare coincident ULS and EM measurements. As can be seen in Figure 3.2.35, ULS and EM data agree well with each other at level ice thicknesses of typically 0.2 to 0.3 m, and can very well distinguish between level and ridged ice. However, there is large disagreement of up to 60 percent in ridge zones. This is further illustrated in Figure 3.2.36, showing a scatter plot of EM versus ULS thickness from Figure 3.2.35. The correlation between both data sets is very good, however, the slope of the linear regression shows that the EM-derived ice thickness is only 0.4 times the ULS ice thickness. Again, this deviation is due to the footprint of the EM method, and due to the unconsolidated nature of the Baltic ridge keels, which were composed of broken, thin ice blocks. In addition, the sensitivity of EM measurements to thickness variations is limited as seawater in the Baltic is only brackish, leading to small conductivity contrasts between the ice and the water. A similar comparison should be performed under arctic conditions to draw final conclusions about the performance of EM measurements over ridges. In principle, the good correlation shown in Figure 3.2.36 and the linear equation provide a means to correct EM measurements over ridges and to make them comparable with ULS measurements.

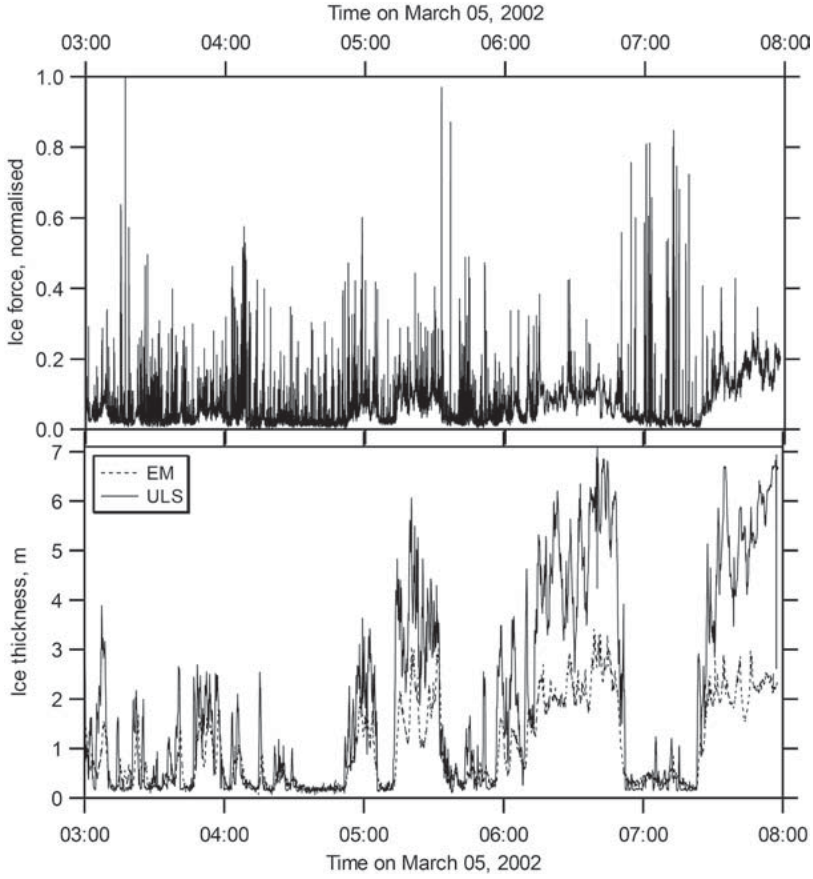

Figure 3.2.35. Typical five-hour time series of forces (top) and ULS and EM ice thicknesses (bottom) for a strong drift event on March 05, 2002 (Haas and Jochmann 2003).

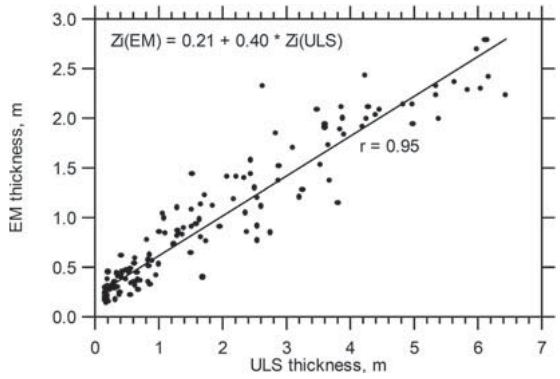

Figure 3.2.36. Comparison of coincident, three-minute average EM and ULS ice thickness measurements from Figure 3.2.35 (Haas and Jochmann 2003).

3.2.9.5 Monitoring tof Ice Thinning and Detection of Weak Points

Understanding of the development of ice thinning during the ablation season is of particular importance for studies of the sea ice mass balance, and for the detection of weak points in the ice cover which could provide a hazard for on-ice travel and the deployment of equipment. Ice mass balance buoys (Section 3.2.6) provide this information with a high accuracy at one location, but many would be required to monitor the thinning along, for example, a skidoo route across the ice. Similarly, ULS profiling could provide information on the thickness change of fast ice, or on the general decrease of mean ice thickness, with limited information on the particular characteristics of the ice, for example, if the melting was stronger over melt ponds or unponded ice. Section 3.2.9.2 has already discussed how extended EM profiles could be obtained to support human activities and various research on the ice. These profiles can of course be repeated throughout the summer season to follow the thinning at different locations along the transects. In addition, EM measurements are nondestructive, leaving hydraulic conditions unchanged once meltponds have developed. In addition, EM measurements are robust against seasonal changes of ice properties and can obtain reliable data even over melt ponds.

Figure 3.2.37 shows an example of such a measurement performed repeatedly along the same profile throughout the summer season (Eicken et al. 2001). The data were obtained during the Surface Heat Budget of the Arctic Ocean (SHEBA) drift station on mixed first- and multiyear ice in the Beaufort Sea. The figure shows the

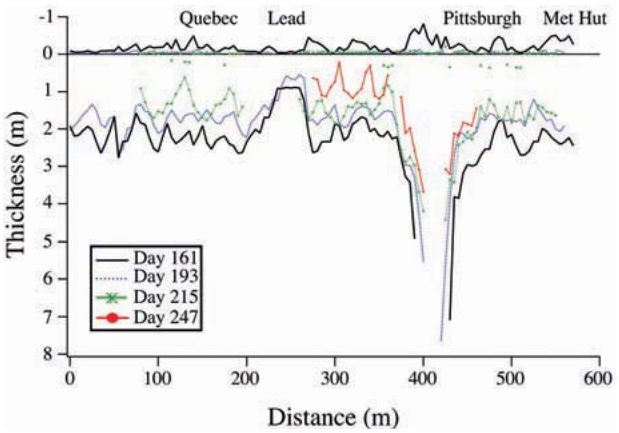

Figure 3.2.37. Repeat EM thickness measurements (5 m spacing) along the same profile during the course of one ablation season between Day 161 (June 10) and Day 247 (Sept. 04) (Eicken et al. 2001). Note that thickness axis points downwards so as to roughly match floe bottom topography. Snow (completely gone by day 193) or melt pond depths (individual points visible below zeroline) are plotted at the top: these are drawn to scale but with reversed sign compared to thickness data. Data missing along the profile later in the season are a result of floe disintegration. Reprinted from the Annals of Glaciology with permission of the International Glaciological Society.

results of four surveys between June and September, and shows the variable thinning at different locations with different ice characteristics. The strongest thinning was observed at the ridge flanks. In addition, the roughness of undeformed ice increases during the summer due to deepening of melt ponds and enhanced bottom melt.

Clearly, these data are invaluable for understanding the mechanisms of summer ice decay. However, measurements can also indicate where regions of enhanced melting or generally thinner ice occur along travel routes over the ice, which can for example also be caused by enhanced under-ice currents. Therefore, these measurements can also help to design better routes and to repeatedly assess their safety.

3.2.10 OUTLOOK

It seems plausible that the retreat of arctic sea ice observed over the last 30 years will continue into the future, thus permitting a dramatic increase in both arctic transportation systems and arctic resource development (Brigham 2007). Such a transformation, regardless of when it may take place, will require more information on ice thickness and morphology. Data gathering may be heavily driven by an immediate need for information on wide ranges of spatial and temporal scales, unprecedented in the historical data sets discussed in this chapter.

Considering, for example, the likely prospect of increased oil and gas activity in the Arctic (AMAP 2007), a dependence on spatially and temporally resolved ice thickness information for planning and monitoring will emerge. This may be needed for standard operations that may use ice as a platform or view it as an encroaching hazard to structures. From the perspective of oil-spill planning and response, ice surface roughness, as determined from laser altimetry for example, may be used as a proxy for under-ice topography, which is important in determining the fate of migrating or pooled oil under ice (Danielson and Weingartner 2007). Another potential growing need of up-to-date ice thickness information will be for arctic search and rescue efforts (e.g., establishing a safe on-ice runway for a C-130 Hercules). Arctic environmental protection efforts may also emerge as users of ice thickness information as environmental assessments and monitoring become critical in mitigating development impacts. Assessments of ice as a habitat for threatened species, such as the polar bear, may also benefit from available data sets.

While current techniques may become operational and more broadly used, such as shipborne EM sounding from both icebreakers and ice-strengthened vessels, novel approaches to more efficiently employ the geophysical principles for remotely determining ice thickness will be undoubtedly explored.

The small- and large-scale spatial and temporal variability of the ice, its relative thinness compared to water depth or the thickness of glacial ice, as well as its mobility require sophisticated methods for its observation. However, these characteristics also prevent the easy application of many classical methods and reduction of their uncertainties. While the accuracies of most methods may be sufficient for

most applications, deployment of sensors is just another challenge as well. Future developments will mainly focus on improved operability, for example by increasing the observational ranges using unmanned aerial and underwater vehicles, or fixed-wing airplanes. Proven methods will be refined, as for example with radar altimetry, which will be operated in high-resolution synthetic aperture radar (SAR) mode of Cryosat (Wingham et al. 2004), to be launched in late 2009. This higher resolution will not only increase the accuracy of sea-surface height retrievals but also result in a higher fraction of ice-only waveforms for the observation of sea ice freeboard (see Section 3.2.8.4). In addition, it can be hoped that space agencies will improve the longevity of observing programs and missions. With this respect, ESA's Sentinel program and NASA's considerations of renewing the ICESat mission are promising efforts. Nevertheless, issues of spatial and temporal resolution have yet to be addressed. In addition, due to both their close physical interaction and their role in determining ice thicknesses from surface elevation or draft, respectively, improved snow thickness estimates are a major task for future developments. The application of any satellite algorithm should be accompanied by extensive ground-truth programs throughout mission lifetimes.

In considering continued needs for ice thickness information and acknowledging that many of the uses of this data have yet to be realized, it is important to accompany performed measurements with as much auxiliary and metadata as possible such that the potential for data use is maximized, especially when considering data that is to be released to the public. Common data protocols and formats should be established, and data storage should be secured in central data archiving centers. Regardless of future arctic climate scenarios, most data collection in the polar regions will continue to prove costly and challenging relative to other areas of the world.

REFERENCES

AMAP (2007), *Arctic Oil and Gas 2007*, Arctic Monitoring and Assessment Programme, Oslo, Norway.

Barker, A., G. Timco, and B. Wright (2006), Traversing grounded rubble fields by foot—Implications for evacuation, *Cold Reg. Sci. Tech., 46,* 79–99.

Björk, G., C. Nohr, B. G. Gustafsson, and A. E. B. Lindberg (2008), Ice dynamics in the Bothnian Bay inferred from ADCP measurements, *Tellus A, 60*(1), 178–188, doi:10.1111/j.1600-0870.2007.00282.x.

Bourke, R. H., and R. P. Garrett (1987), Sea ice thickness distribution in the Arctic Ocean, *Cold Reg. Sci. Technol., 13,* 259–280.

Brigham, L. W. (2007), Thinking about the Arctic's future: Scenarios for 2040, *The Futurist*, September–October, 27–34.

Danielson, S. E., and T. J. Weingartner (2007), Estimates of Oil spill dispersion extent in the Nearshore Alaska Beaufort Sea based on in-situ oceanographic

measurements, *ADEC Division of Spill Prevention and Response*, Anchorage, Alaska.

Dierking, W. (1995), Laser profiling of the ice surface topography during the Winter Weddell Gyre Study 1992, *J. Geophys. Res., 100*(C3), 4807–4820.

Dowdeswell, J. A., J. Evans, R. Mugford, G. Griffiths, S. McPhail, N. Millard, P. Stevenson, M. A. Brandon, C. Banks, K. J. Heywood, M. R. Price, P. A. Dodd, A. Jenkins, K. W. Nicholls, D. Hayes, E. P. Abrahamsen, P. Tyler, B. Bett, D. Jones, P. Wadhams, J. P. Wilkinson, K. Stansfield, and S. Ackley (2008), Autonomous underwater vehicles (AUVs) and investigations of the ice-ocean interface: Deploying the Autosub AUV in Antarctic and Arctic waters. *J. Glac.,* 54(187), pp. 661–672.Eicken, H., A.L. Lovecraft, and M.L. Druckenmiller (2009), Sea Ice System Services: A Framework to Help Identify and Meet Information Needs Relevant for Arctic Observing Networks, Arctic 62(2), in press.

Eicken, H., W. B. Tucker, and D. K. Perovich (2001), Indirect measurements of the mass balance of summer Arctic sea ice with an electromagnetic induction technique, *Ann. Glaciol., 33,* 194–200.

Fetterer, F.M., M.R. Drinkwater, K.C. Jezek, S.W.C. Laxon, R.G. Onstott, and L. M. H. Ulander (1992), Sea ice altimetry, in *Microwave Remote Sensing of Sea Ice*, *Geophysical Monograph*, *68*, pp. 111–135, American Geophysical Union, Washington, DC.

Forsberg, R., and H. Skourup (2005), Arctic Ocean gravity, geoid and sea ice freeboard heights from ICESat and GRACE, *Geophys. Res. Lett., 32*, L21502, doi:10.1029/2005GL023711.

Granberg, H. B., and M. Leppäranta (1999), Observations of sea ice ridging in the Weddell Sea, *J. Geophys. Res., 104*(C11), 25,735–25,745.

George, J. C., H. P. Huntington, K. Brewster, H. Eicken, D. W. Norton, and R. Glenn (2004), Observations on shorefast ice dynamics in Arctic Alaska and the responses of the Iñupiat hunting community, *Arctic, 57*, 363–374.

Haas, C. (1998), Evaluation of ship-based electromagnetic-inductive thickness measurements of summer sea ice in the Bellingshausen and Amundsen Seas, Antarctica, *Cold Regions Science and Technology, 27*, 1–16.

Haas, C. (2004), Airborne EM sea ice thickness profiling over brackish Baltic sea water, Proceedings of the 17th international IAHR symposium on ice, June 21-25, 2004, vol. 2, pp. 12–17, All-Russian Research Institute of Hydraulic Engineering (VNIIG), Saint Petersburg, Russia.

Haas, C., S. Gerland, H. Eicken, and H. Miller (1997), Comparison of sea ice thickness measurements under summer and winter conditions in the Arctic using a small electromagnetic induction device, *Geophysics, 62*(3), 749–757.

Haas, C., and P. Jochmann (2003), Continuous EM and ULS thickness profiling in support of ice force measurements, in *Proceedings of the 17th International Conference on Port and Ocean Engineering under Arctic Conditions, POAC '03*, Trondheim, Norway, vol. 2, edited by S. Loeset, B. Bonnemaire, and

M. Bjerkas, pp. 849–856, Department of Civil and Transport Engineering, Norwegian University of Science and Technology NTNU, Trondheim, Norway.

Haas, C., A. Pfaffling, S. Hendricks, L. Rabenstein, J.-L. Etienne, and I. Rigor (2008a), Reduced ice thickness in Arctic Transpolar Drift favors rapid ice retreat, *Geophys. Res. Lett., 35,* L17501, doi:10.1029/2008GL034457.

Haas, C., J. Lobach, S. Hendricks, L. Rabenstein, and A. Pfaffling (2008b), Helicopter-borne measurements of sea ice thickness, using a small and lightweight, digital EM system, *J. Appl. Geophys.*, http://dx.doi.org/10.1016/j.jappgeo.2008.05.005.

Haas, C., M. Nicolaus, S. Willmes, A. Worby, and D. Flinspach (2008c), Sea ice and snow thickness and physical properties of an ice floe in the western Weddell Sea and their changes during spring warming, *Deep Sea Research II, 55*(8–9), 963–974, doi:10.1016/j.dsr2.2007.12.020.

Haas, C., K.-H. Rupp, and A. Uuskallio (1999), Comparison of along track EM ice thickness profiles with ship performance data, *POAC '99: Proc 15th Int Conf on Port and Ocean Engineering Under Arctic Conditions*, edited by J. Tuhkuri and K. Riska, vol. 1, pp. 343–353, Helsinki Univ. Techn., Ship Lab., Espoo, Finland.

Hibler, W. D. (1972), Removal of aircraft altitude variation from laser profiles of the Arctic ice pack, *J. Geophys. Res., 77*(36), 7190–7195.

Hibler, W. D. (1975), Characterization of cold-regions terrain using airborne laser profilometry, *J. Glaciol., 15*(73), 329–347.

Holt, B., P. Kanagaratnam, S.P. Gogineni, V. C. Ramasami, A. Mahoney, and V. Lytle (2008), Sea ice thickness measurements by ultrawideband penetrating radar: First results, *Cold Reg. Sci. Technol.,* doi:10.1016/ j.coldregions.2008.04.007.

Hvidegaard, S. M., and R. Forsberg (2002), Sea ice thickness from airborne laser altimetry over the Arctic Ocean north of Greenland, *Geophys. Res. Lett., 29*(20), 1952, doi:10.1029/2001GL014474.

Hvidegaard, S. M., R. Forsberg, and H. Skourup (2006), Sea ice thickness estimates from airborne laser scanning, in Arctic sea ice thickness: Past, present and future, in *Climate Change and Natural Hazard Series*, vol. 10, edited by P. Wadhams and G. Amanatidis, pp. 193–206, European Commission, Brussels.

Kanagaratnam, P., T. Markus, V. Lytle, B. Heavey, P. Jansen, G. Prescott, and S. P. Gogineni (2007), Ultrawideband radar measurements of thickness of snow over sea ice, *Trans. Geosci. Remote Sens., 45*(9), 2715–2724.

Kovacs, A., J. S. Holladay, and C. J. J. Bergeron (1995), The footprint/altitude ratio for helicopter electromagnetic sounding of sea ice thickness: comparison of theoretical and field estimates, *Geophysics, 60*, 374–380.

Kovacs, A., and R. M. Morey (1986), Electromagnetic measurements of multi-year sea ice using impulse radar, *Cold Reg. Sci. Tech., 12,* 67–93.

Kovacs, A., and R. M. Morey (1991), Sounding sea ice thickness using a portable electromagnetic induction instrument, *Geophysics, 56,* 1992–1998.

Kovacs, A., N. C. Valleau, and J. S. Holladay (1987a), Airborne electromagnetic sounding of sea ice thickness and subice bathymetry, *Cold Regions Sci. and Tech., 14*, 289–311.

Kovacs, A., R. M. Morey, G. F. N. Cox, and N. C. Valleau (1987b), Electromagnetic property trends in sea ice, Part 1, *CRREL Report*, vol. 87–6, U.S. Army Cold Regions and Engineering Laboratory, Hanover, NH.

Kwok, R., G. F. Cunningham, H. J. Zwally, and D. Yi (2006), ICESat over Arctic sea ice: Interpretation of altimetric and reflectivity profiles, *J. Geophys. Res., 111*, C06006, doi:10.1029/2005JC003175.

Kwok, R., and G. F. Cunningham (2008), ICESat over Arctic sea ice: Estimation of snow depth and ice thickness, *J. Geophys. Res., 113*, C08010, doi:10.1029/2008JC004753.

Kwok R., G. F. Cunningham, H. J. Zwally, and D. Yi (2007), Ice, Cloud, and land Elevation Satellite (ICESat) over Arctic sea ice: Retrieval of freeboard, *J. Geophys. Res., 112*, C12013, doi:10.1029/2006JC003978.

Lange, M. A., and H. Eicken (1991), The sea ice thickness distribution in the northwestern Weddell Sea, *J. Geophys. Res., 96*(C3), 4821–4837.

Laxon, S., N. Peacock, and D. Smith (2003), High interannual variability of sea ice thickness in the Arctic region, *Nature, 425*, 947–950, doi:10.1038/nature02050.

Liu, G., and A. Becker (1990), Two-dimensional mapping of sea ice keels with airborne electromagnetics, *Geophysics, 55*, 239–248.

Mahoney, A., H. Eicken, and L. Shapiro (2007), How fast is landfast ice? A study of the attachment and detachment of nearshore ice at Barrow, Alaska, *Cold Reg. Sci. Tech., 47,* 233–255.

Mahoney, A., and S. Gearheard (2008), Handbook for community-based sea ice monitoring, *NSIDC Special Report*, vol. 14, Boulder, CO, U.S. National Snow and Ice Data Center,accessed electronically at http://nsidc.org/pubs/special/nsidc_special_report_14.pdf.

McNeill, J. D. (1980), Electromagnetic terrain conductivity measurements at low inductions numbers, *Technical Note TN-6*, Geonics Limited, Mississauga, Ontario, accessed electronically, http://www.geonics.com/pdfs/technical-notes/ tn6.pdf.

Melling, H., P. H. Johnston, and D. A. Riedel (1995), Measurement of the topography of sea ice by moored subsea sonar, *J. Atmosph. Oceanic Techn., 12*(3), 589–602.

Melling, H. (1998), Sound scattering from sea ice: Aspects relevant to ice-draft profiling by sonar, *J. Atmosph. Oceanic Technol., 15,* 1023–1034.

Melling, H. (2002), Sea ice of the northern Canadian Arctic Archipelago, *J. Geophys. Res., 107*(C11), 3181, doi:10.1029/2001JC001102, 2002.

Melling, H., D. A. Riedel, and Z. Gedalof (2005), Trends in the draft and extent of seasonal pack ice, Canadian Beaufort Sea, *Geophys. Res. Lett., 32*, L24501,

doi:10.1029/2005GL024483.

Multala, J., H. Hautaniemi, M. Oksama, M. Leppäranta, J. Haapala, A. Herlevi, K. Riska, and M. Lensu (1996), An airborne electromagnetic system on a fixed wing aircraft for sea ice thickness mapping, *Cold Reg. Sci. Techn., 16*(24), 355–373.

Mock, S. J., A. D. Hartwell, and W. D. Hibler (1972), Spatial aspects of pressure ridge statistics, *J. Geoph. Res., 77*(30), 5945–5953.

Otto, D. (2004), Validation of ground-penetrating radar measurements of first- and multiyear sea ice and snow thickness in the Arctic and Antarctic, Diploma thesis (in German), Alfred Wegener Institute of Polar and Marine Research, Bremerhaven, Germany, and Geophysical Institute, Technical University Clausthal, Germany.

Peacock, N. R., and S. W. Laxon (2004), Sea surface height determination in the Arctic Ocean from ERS altimetry, *J. Geophys. Res., 109*, C07001, doi:10.1029/2001JC001026.

Perovich, D. K., T. C. Grenfell, J. A. Richter-Menge, B. Light, W. B. Tucker III, and H. Eicken (2003), Thin and thinner: Sea ice mass balance measurements during SHEBA, *J. Geophys. Res., 108*(C3), 8050, doi:10.1029/2001JC001079, 2003.

Pfaffling, A., C. Haas, and J. E. Reid (2007), A direct helicopter EM sea ice thickness inversion, assessed with synthetic and field data, *Geophysics, 72*, F127–F137.

Potter, R. E., and J. T. Walden (1981), Design and construction of sea ice roads in the Alaskan Beaufort Sea. *Proceedings of the 13th Annual Offshore Technology Conference*, Houston, Texas, pp. 135–140.

Prinsenberg, S. J., and J. S. Holladay (1993), Using air-borne electromagnetic ice thickness sensor to validate remotely sensed marginal ice zone properties, *Port and Ocean Engineering under Arctic Conditions (POAC 93)*, vol. 2, pp. 936–948, edited by Hamburger Schiffbau Versuchsanstalt (HSVA), Hamburg, Germany.

Prinsenberg, S. J., J. S. Holladay, and J. Lee (2002), Measuring ice thickness with EISFlowTM, a fixed-mounted helicopter electromagnetic-laser system, in *Proceedings of the Twelfth (2002) International Offshore and Polar Engineering Conference May 26–May 31, 2002*, vol. 1, pp. 737–740, Kitakyushu, Japan.

Reid, J. E., A. Pfaffling, and J. Vrbancich (2006), Airborne electromagnetic footprints in 1D earths, *Geophysics, 71*, G63–G72.

Richter-Menge, J. A., D. K. Perovich, B. C. Elder, K. Claffey, I. Rigor, and M. Ortmeyer, (2006), Ice mass balance buoys: A tool for measuring and attributing changes in the thickness of the Arctic sea ice cover, *Ann. Glaciol., 44*, 205–210.

Rossiter, J. R., and J. S. Holladay (1994), Ice-thickness measurement, in *Remote Sensing of Sea Ice and Icebergs,* edited by S. Haykin et al., pp. 141–176, John Wiley, Hoboken, NJ.

Rothrock, D. A., D. B. Percival, and M. Wensnahan (2008), The decline in arctic sea ice thickness: Separating the spatial, annual, and interannual variability in a quarter century of submarine data, *J. Geophys. Res., 113*, C05003, doi:10.1029/2007JC004252.

Rothrock, D. A. and M. Wensnahan (2007), The accuracy of sea ice drafts measured from U.S. Navy submarines, *J. Atmos. Oceanic Technol.,* doi:10.1175/JTECH2097.1.

Rothrock, D. A., Y. Yu, and G. A. Maykut (1999), Thinning of the Arctic sea ice cover, *Geophys. Res. Lett., 26*(23), 3469–3472.

Shcherbina, A. Y., D. L. Rudnick, and L. D. Talley (2005), Ice-draft profiling from bottom-mounted ADCP data, *J. Atmosph. Oceanic Techn., 22,* 1249–1266.

Skourup, H., and R. Forsberg (2006), Sea ice freeboard from ICESat: A comparison with airborne lidar measurements, in *Arctic Sea Ice Thickness: Past, Present, and Future*, Climate Change and Natural Hazard Series, vol. 10, edited by P. Wadhams and G. Amanatidis, pp. 82–92, European Commission, Brussels.

Sodhi, D. S., D. B. Griggs, and W. B. Tucker, (2001), Ice performance tests of the USCGC Healy, *POAC '01: Proceedings of the 16th International Conference on Port and Ocean Engineering under Arctic Conditions*, vol. 2, edited by R. Frederking, I. Kubat, and G. Timco, pp. 893–907, Canadian Hydraulics Center, National Research Council, Ottawa, Ontario

Stogryn, A., and G. J. Desargant (1985), The dielectric properties of brine in sea ice at microwave frequencies, *IEEE Trans. on Antennas and Propagation, AP-33*, 523–532.

Strass, V. H., and E. Fahrbach (1998), Temporal and regional variation of sea ice draft and coverage in the Weddell Sea obtained from upward looking sonars, in *Antarctic Sea Ice: Physical Processes, Interactions, and Variability*, Antarctic Research Series, vol. 74, edited by M. O. Jeffries, pp. 123–139, American Geophysical Union, Washington, DC.

Sun, B., J. Wen, M. He, J. Kang, Y. Luo, and Y. Li (2003), Sea ice thickness measurement and its underside morphology analysis using radar penetration in the Arctic Ocean, *Sci. China, 46*(11), 1151–1160.

Thorndike, A. S., D. A. Rothrock, G. A. Maykut, and R. Colony (1975), The thickness distribution of sea ice, *J. Geophys. Res., 80*(33), 4501–4513.

Vinje, T., N. Nordlund, and Å. Kvambekk (1998), Monitoring ice thickness in Fram Strait, *J. Geophys. Res., 103*(C5), 10,437–10,449.

Wadhams, P., and N. R. Davis (2000), Further evidence of ice thinning in the Arctic Ocean, *Geophys. Res. Lett., 27*(24), 3973–3975.

Wadhams, P., M. A. Lange, and S. F. Ackley (1987), The ice thickness distribution across the Atlantic sector of the Antarctic Ocean in midwinter, *J. Geophys. Res., 92*(C13), 14,535–14,552.

Wadhams, P., W. B. Tucker III, W. B. Krabill, R. N. Swift, J. C. Comiso, and N. R. Davis (1992), Relationship between sea ice freeboard and draft in the Arctic

Basin, and implications for ice thickness monitoring, *J. Geophys. Res., 97*(C12), 20,325–20,334.

Wadhams, P., J. P. Wilkinson, and S. D. McPhail (2006), A new view of the underside of Arctic sea ice, *Geophys. Res. Lett., 33*, L04501, doi:10.1029/2005GL025131.

Warren, S. G., I. G. Rigor, N. Untersteiner, V. F. Radionov, N. N. Bryazgin, Y. I. Aleksandrov, and R. Colony (1999), Snow depth on Arctic sea ice, *J. Clim., 12,* 1814–1829, doi:10.1175/1520-0442(1999)012<1814:SDOASI > 2.0.CO;2.

Wingham, D. J., L. Phalippou, C. Mavrocordatos, and D. Wallis (2004), The mean echo and echo cross product from a beamforming interferometric altimeter and their application to elevation measurement, *IEEE Trans. Geosci. Rem. Sens., 42*(10), 2305–2323, doi:10.1109/TGRS.2004.834352.

Worby, A. P., C. A. Geiger, M. J. Paget, M. L. Van Woert, S. F. Ackley, and T. L. DeLiberty (2008), Thickness distribution of Antarctic sea ice, *J. Geophys. Res., 113*, C05S92, doi:10.1029/2007JC004254.

Worby, A. P., M. O. Jeffries, W. F. Weeks, K. Morris, and R. Jaña (1996), The thickness distribution of sea ice and snow cover during late winter in the Bellingshausen and Amundsen Seas, Antarctica, *J. Geophys. Res., 101*(C12), 28,441–28,455.

Zwally, H. J., B. Schutz, W. Abdalati, J. Abshire, C. Bentley, A. Brenner, J. Bufton, J. Dezio, D. Hancock, D. Harding, T. Herring, B. Minster, K. Quinn, S. Palm, J. Spinhirne, and R. Thomas (2002), ICESat's laser measurements of polar ice, atmosphere, ocean, and land, *J. Geodyn., 34*, 405–445, doi:10.1016/S0264-3707(02)00042-X.